BB

GSI

GAMOW-TELLER BETA DECAY AND THE STRUCTURE OF NUCLEI NEAR THE DOUBLY-MAGIC NUCLEUS $^{100}_{50}Sn_{50}$

K. RYKACZEWSKI

Scu9S34

Gamow–Teller Beta Decay
and the Structure of Nuclei
near the Doubly–Magic Nucleus
$^{100}_{50}Sn_{50}$

Krzysztof Rykaczewski

Institute of Experimental Physics

Warsaw University

Pl-00-681 Warszawa, Hoża 69

Poland

Warszawa, 1995

Contents

1 Introduction

This paper reviews the results of experiments on the beta decay and of relevant theoretical studies for nuclides in the region of doubly magic ^{100}Sn.

Studies of doubly closed-shell nuclides and neighbouring isotopes are very important for testing nuclear models, as the model description of such nuclei can be based on the coupling of a few particles and/or holes to the $I^{\pi} = 0^{+}$ doubly-magic core. Main properties of nuclear states like e.g. spin and parity reflect the presence and interaction of these few active orbitals only. Measurements and interpretation of the transition rates occuring at "doubly-magic sites" allow for a deeper insight into the structure of nuclei involved. This applies in particular to the allowed beta transitions, which are specially selective due to the very stringent selection rules.

The doubly-magic nuclides having the same number of protons and neutrons $(Z = N)$ are especially well suited for nuclear structure studies. Since the protons and neutrons occupy the same orbits, the spatial parts of the wave functions are identical and the isospin dependence of the nuclear interaction can be well tested. There are only five $N = Z$ doubly-magic nuclei: stable ^{4}He, ^{16}O and ^{40}Ca, and radioactive ^{56}Ni and ^{100}Sn. The latter one has been recently identified in the projectile fragment separator based experiments at GSI Darmstadt [1] and GANIL Caen [2, 3]. The next candidate ^{164}Pb is an unbound system according to all recent mass predictions, see e.g. [4].

^{100}Sn lies very far off the line of beta stability, with the deficit of neutrons with respect to the mean atomic mass of the stable tin isotopes exceeding 18. It makes this doubly-magic nucleus and its closest neighbours difficult to reach experimentally but very attractive for beta decay studies. Beta decay data allow a meaningfull verification of model predictions as, due to the high decay energy values typical for nuclides far from stability, the distribution of transition strength can be determined in a large energy interval [5, 6].

The beta decay in the ^{100}Sn region is dominated by an allowed Gamow-Teller (GT) transformation of a $g_{9/2}$ proton into a $g_{7/2}$ neutron, see chapter 2. Within elementary single-particle shell model (ESPSM), these two orbits are expected to be always responsible for the decay, even if the relevant configuration is distributed over many levels due to residual interactions. This great simplicity of the shell-model picture of the decay is of particular importance. Identification of a fast beta transition leads to an unambiguous interpretation, and even limited amount of data can be used to verify

3

theoretical calculations. The analysis of these data with reference to model predictions eventually allows one to determine the degree of renormalization of the axial vector coupling constant g_A with respect to the free neutron value.

This was a motivation for a series of experiments carried out at GSI Darmstadt [7, 8], CERN/ISOLDE [9, 10], LISOL Louvain–la–Neuve and most recently GANIL Caen [11], followed by a number of theoretical studies performed within nuclear structure models [12–23]. Beta decay properties of several nuclei in the ^{100}Sn region have been measured for the first time establishing a systematics of experimental data on the distribution and magnitude of the $\pi g_{9/2} \rightarrow \nu g_{7/2}$ GT–transformation strength (see chapter 3). It was demonstrated that the ESPSM overestimates the expected GT–strength typically by a factor of five, and strongly underestimates the number of levels populated in daughter nuclides. Since only part of the strength reduction can be accounted for by core polarisation effects in the parent nuclei, a more detailed analysis of the nuclear structure of the states involved in the decay process has been made. In particular, a satisfactory description of the observed splitting of the GT–transitions has been achieved within advanced large space shell–model calculations (see chapter 4). This has allowed to estimate the amount of the GT–strength missed due to the limited Q_{EC} observation window as well as due to limited experimental sensitivity. The theoretically expected total GT–decay strengths, obtained by summing over the individual transitions, are much closer to the corresponding experimental values than the ESPSM predictions, see chapter 4. However, a good agreement is achieved only after a reduction of g_A with respect to the free–neutron value by about 20%.

Concerning the origin of this g_A reduction observed, the experimental and theoretical results presented in this survey show that an explanation related to the restrained observation windows seems unlikely at least for the most neutron–deficient nuclides investigated. This is an important result of the studies performed until now. A detailed study of the ^{100}Sn decay would represent a very important extension of these investigations. This decay scheme is predicted to be extremely simple. One may expect that a careful study of the ^{100}Sn activity, when its production rate will be high enough, will bring an essential contribution to our knowledge of the g_A renormalization in heavy nuclei.

If the experimental origin of the GT strength reduction were definitely excluded, a possible shift of a part of this strength to very high energies, unaccounted for in the standard model approaches, should be considered (see chapter 4). Such a shift could

be connected to higher order tensor interactions between nucleons [24, 25, 26, 27] or to a fascinating possibility involving Δ–resonances [28–35]. The latter would mean that the renormalization of g_A in nuclear matter has to be related, at least partly, to subnucleonic degrees of freedom. This problem has been also studied via 'reverse beta–decay', namely (p, n) and (n, p) reactions, see e.g. [33, 34]. However, such studies are limited to stable targets. Moreover, the separation between effect and background in such experiments is not as unambiguous as in the background–free data obtained by using very selective allowed beta decay. These investigations are not reviewed here.

For a more stringent verification of nuclear models, the information on the beta decay reported here should be combined with the results of in–beam studies [36] that yield data on higher spin states in nuclei near ^{100}Sn. However, this is beyond the scope of the present review. Also the interesting problem of the relation between the decay properties of neutron–deficient nuclides with $Z \approx N$ below ^{100}Sn and the path of the rapid proton capture in stellar environments [37, 38] is omitted here.

The GT decay of heavy nuclides, and relevant nuclear structure aspects, had also been studied in the ^{146}Gd region. The investigated nuclei in this region are closer to the beta–stability line and thus easier to produce. Rich and important results [39, 40] have been obtained, in particular on the $\pi h_{11/2} \rightarrow \nu h_{9/2}$ GT–transformation [41, 42, 43]. However, the efforts to reach and study ^{100}Sn and its closest neighbours are still well justified. In particular, the doubly–magic character of ^{100}Sn is expected to be much more pronounced than that of ^{146}Gd. The neutron energy gaps for $N = 50$ and $N = 82$ are similarly large, about 6 to 7 MeV, and 5 to 6 MeV, respectively. However, the proton energy gap for $Z = 50$ separates the $\pi g_{9/2}$ orbital from the next $\pi g_{7/2}$ one by as much as 6 MeV, while the $Z = 64$ subshell–closure corresponds to about 2 MeV. Also, it is important to note that three proton orbitals, i.e. $\pi h_{11/2}$, $\pi s_{1/2}$ and $\pi d_{3/2}$, are almost at the same energy for nuclei above ^{146}Gd. This reduces the proton occupation of the $\pi h_{11/2}$ orbital, and consequently the observed strength of the $\pi h_{11/2} \rightarrow \nu h_{9/2}$ GT–transition. The energy windows (Q_{EC}) for the beta decay in the ^{100}Sn region are on average a few MeV higher than the corresponding values for nuclei studied in the ^{146}Gd region. Last but not least, the nuclides near ^{100}Sn are close to the proton drip line and their structure is expected to reveal the effects related to the coupling between bound states and the particle continuum. As emphasized by Nazarewicz *et al* [44], this is one of the most exciting challenges in nuclear physics today.

2 Beta Decay near ^{100}Sn

2.1 Fermi and Gamow–Teller Decay

The weak interactions occurring in nuclei are responsible for the beta decay. For nuclei far from stability, the most probable, dominating decay channels are attributed to the allowed transitions of Fermi (F) and Gamow–Teller (GT) type [45].

For a Fermi transition, the interaction operator F acts only on the isospin part of the wave function. The spatial part of this function must be the same in the initial and final state. The projection of isospin T_Z changes by ± 1 (proton$\leftrightarrow$neutron), while the isospin T remains unchanged. Hence, fast Fermi transitions are possible only between isobaric analog states (IAS). They have been observed mainly for relatively light neutron–deficient nuclides, where the energy condition $Q_{EC} \geq E_F$ is fulfilled. Here E_F is equal to the Coulomb energy difference between the initial and final nucleus, corrected for the mass difference of 0.782 MeV between neutron and hydrogen atom. For $0^+ \rightarrow 0^+$ beta transitions only the Fermi transformation is possible, see Table 1. Transitions between mirror nuclei are examples of a mixed Fermi and Gamow–Teller decay [46, 47].

The Gamow–Teller operator acts not only on the isospin, but also on the spin degrees of freedom. Examples of GT beta decay may be found all over the chart of nuclei. Among the best experimentally and theoretically studied nuclei are those of the sd–shell [48, 49, 50, 51, 52]. Particularly interesting are the regions where Fermi decay is energetically forbidden and the GT transformation is the only allowed channel. This holds e.g. for nuclei near the doubly–magic nucleus ^{100}Sn, with large proton excess (as compared to the stable systems). In this region, E_F exceeds 13 MeV, while Q_{EC} values of nuclides that have been studied until now are predicted to be lower than that. It means that our considerations of allowed beta decay in this region may be restricted to GT decay (a drip–line nucleus ^{94}Ag might be an exception [53]).

The compilation of the selection rules and typical comparative half–life values ft for Fermi and Gamow–Teller decays is given in Table 1 (for more details see e.g. a recent textbook of Grotz and Klapdor–Kleingrothaus [45] on weak interactions).

6

Table 1: Selection rules for allowed β–transitions.

Beta transition	Transition Operator	Spin I	Orbital angular momentum l Parity π	Isospin T	Coupling constant	Typical $\log(ft)$
Fermi	τ	$\Delta I = 0$	$\Delta l = 0,$ $\Delta \pi = 0$	$\Delta T = 0$	g_V	≈ 3.5
Gamow- –Teller	$\sigma\tau$	$\mid \Delta I \mid = 0, 1$ no $0 \to 0$	$\Delta L = 0,$ $\Delta \pi = 0$	$\mid \Delta T \mid = 0, 1$	g_A	$\approx 3 - 6$

The comparative half–life value ft (where f is a phase space factor, i.e. the well known function of a beta transition energy, tabulated for a given element in [54, 55], and where $t = T_{1/2}/I_\beta$ is the partial half–life for a beta transition of intensity I_β per decay) is related to the nuclear matrix element between initial and final state of the allowed beta transitions $M_F = < \tau >$ and $M_{GT} = < \sigma\tau >$

$$ft = \frac{6147}{M_F^2 + (\frac{g_A}{g_V})^2 M_{GT}^2} \quad . \tag{1}$$

The constant 6147 ± 7 s is available from the evaluation of the experimental data on $0^+ \to 0^+$ superallowed beta decays [56], and the ratio of vector to axial vector coupling constants has its free neutron value of $g_A/g_V = -1.262 \pm 0.004$ [57, 58].

In a recent reexamination of the data on the superallowed beta decays [47] a value of 6127 ± 10 s was suggested for the constant in formula (1). Also for the g_A/g_V ratio more recent result of -1.2544$\pm$0.0036 exists in the literature [59]. However, both these numbers are outside of the $\pm 1\sigma$ error bar limits when compared to earlier evaluations, and they have to be critically reanalysed before adopting. For a given matrix element, the variation of the ft values due to variations in the values of these constants is below 1%.

The strength $B(GT)$ of a GT transition is equal to the square of transition matrix element

$$B(GT) = M_{GT}^2 = < final\,state \mid \sigma\tau \mid initial\,state >^2 \qquad . \qquad (2)$$

In particular, when a single particle from a $j_> = l + 1/2$ orbital is transformed into $j_< = l - 1/2$ one, the transition strength $B^{sp}(GT)$ is related [60] to the orbital angular momentum l via simple equation

$$B^{sp}(GT) = < j_< \mid \sigma\tau \mid j_> >^2 = \frac{4l}{2l + 1} \qquad , \qquad (3)$$

where the result is given in $g_A^2/(4\pi)$ units ($\mid g_A \mid = 1.119 \cdot 10^{-4} \text{MeV·fm}^3$).

2.2 Structure of Nuclei near ^{100}Sn and the $\pi g_{9/2} \rightarrow \nu g_{7/2}$ GT–Transformation

New nuclides in the ^{100}Sn region, that have been experimentally identified within the present studies, are given in Fig.1 with respect to the magic numbers N = 50 and Z = 50 and the proton (two–proton) drip line.

It is worth to notice that already quite a number of exotic drip–line nuclei have been reached and partially studied. The region of known isotopes is extended to the predicted [4] proton drip–line for indium and silver isotopes, and even beyond it for antimony and rhodium. A tentative evidence for an existence of ^{105}Te, ^{99}Sn and ^{93}Ag was obtained [3]. The effects related to magic nucleon numbers N = 50 and Z = 50, established for stable and close to stable nuclei, can be tested now far off the beta stability line.

The proton and neutron orbitals relevant to the structure of nuclei in the ^{100}Sn region are given in Fig.2. According to the present knowledge [36], the N = 50 and Z = 50 energy gaps amount to 6.8 and 5.9 MeV, respectively. While filling the $1g_{9/2}$ level with protons, see sequence of the orbitals displayed in Fig.2, one follows the elements from niobium (Z = 41) to tin (Z = 50). Neutron orbits $2d_{5/2}$ and $1g_{7/2}$ are getting occupied when crossing the N = 50 line. They are energetically quite close to each other, almost degenerated according to the present understanding of the nuclear structure in this region [19, 20, 36]. The energies of single–particle levels were mostly determined from

data derived from "in-beam" experiments [36]. However, the decay studies also contributed directly to these input parameters in shell–model calculations, e.g. with a recent observation of the $\pi p_{1/2}$ isomeric states above the $\pi g_{9/2}$ ground–state in the odd–Z elements like indium and silver [61].

Figure 1: Chart of nuclei near the doubly–magic nucleus $^{100}_{50}\text{Sn}_{50}$. New isotopes identified in course of the presented studies are marked by the inclined mass numbers. The mass numbers of the most neutron–deficient isotope of cadmium and tellurium known–to–date are also displayed.

The beta decay of neutron–deficient nuclei situated "south–east" of ^{100}Sn ($Z\leq50$, $N\geq50$, compare Fig.1) is clearly dominated by one allowed transition. This is a GT transformation $\pi g_{9/2} \rightarrow \nu g_{7/2}$, see Fig.2. Here the Fermi beta transition ($\Delta T = 0$), which would transform a proton into a neutron, is excluded due to the limit imposed by the decay energy window.
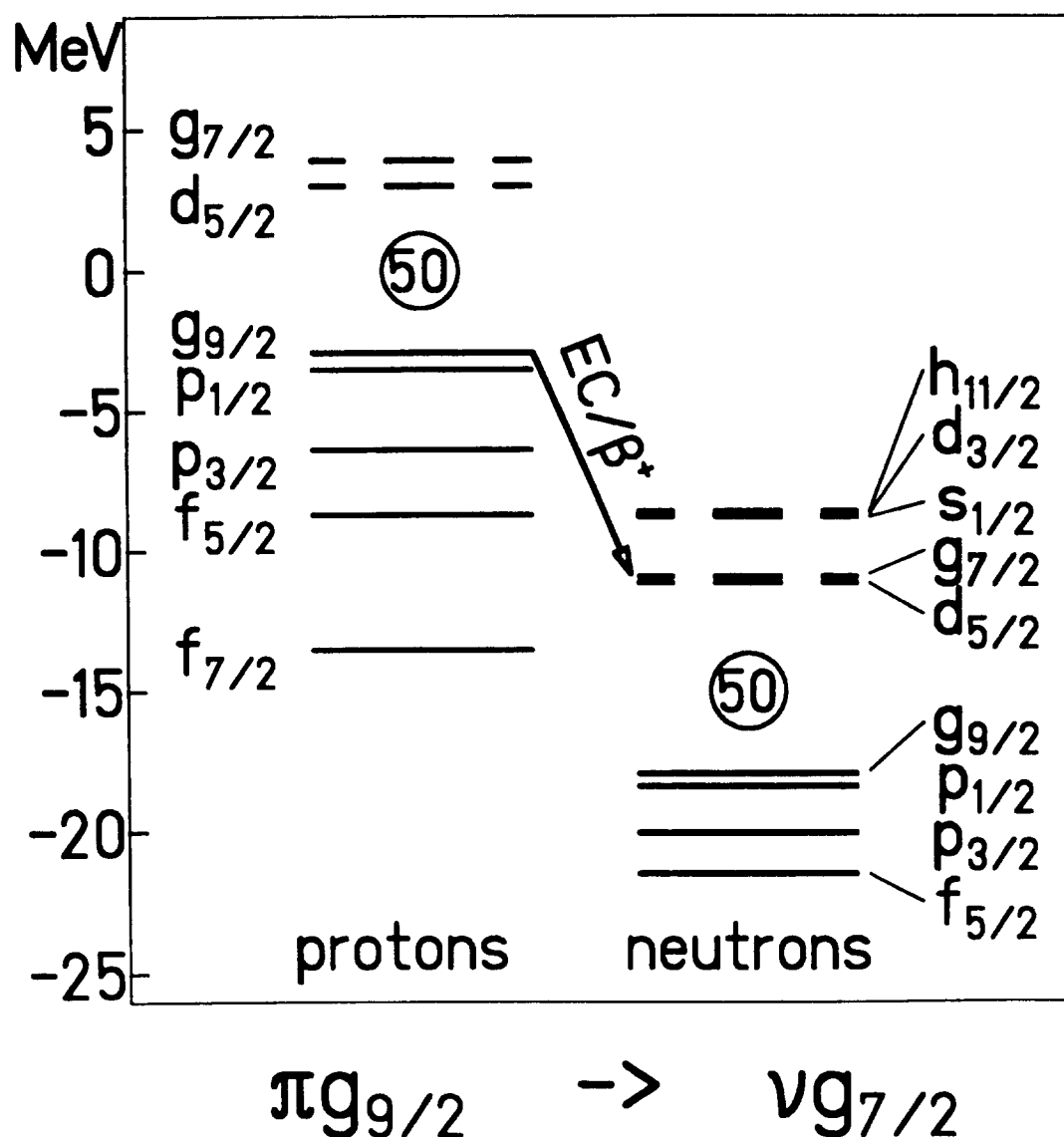
MeV

$g_{7/2}$
$d_{5/2}$

50

$g_{9/2}$
$p_{1/2}$

$p_{3/2}$

$f_{5/2}$

$f_{7/2}$

EC/β_+

$h_{11/2}$
$d_{3/2}$
$s_{1/2}$
$g_{7/2}$
$d_{5/2}$

50

$g_{9/2}$
$p_{1/2}$

$p_{3/2}$
$f_{5/2}$

protons   neutrons

$\pi g_{9/2} \quad \rightarrow \quad \nu g_{7/2}$

Figure 2: Energies of single particle orbitals for doubly–magic nucleus ^{100}Sn. The experimental and "shell–model extrapolated" values [36] are given. The GT beta transition $\pi g_{9/2} \rightarrow \nu g_{7/2}$ occuring in the ^{100}Sn region is also indicated.

Other energetically possible GT channels like e.g. $\pi f_{7/2} \to \nu f_{5/2}$, see Fig.2, are blocked because of the Pauli principle. The $\nu f_{5/2}$ orbit is fully occupied for nuclei in the ^{100}Sn region and the $f_{7/2}$ proton cannot be transformed into a $f_{5/2}$ neutron.

The states fed in the GT beta decay of nuclides near ^{100}Sn should have a relatively simple quasiparticle character [5], in contrast to the levels expected to be populated on the neutron–rich side in the decays of e.g. ^{132}Sn [62] or ^{78}Ni [63, 64]. For the latter nuclei the collective state (Gamow–Teller Resonance), which could be connected with the ground–state of the parent nucleus via the GT–transition taking almost the full GT–strength, is outside the β–decay energy window. For a few nuclei close to ^{100}Sn, according to simple as well as advanced models, most of the GT–strength is expected to be within the decay energy window.

The interpretation is particularly simple for the decay of even–even nuclides where the beta decay process occurs between the 0^+ ground state and the 1^+(one–hole, one–particle) excited level in the final nucleus :

$$0^+(\text{even–even core}) \to 1^+(\pi g_{9/2}^{-1}, \nu g_{7/2}),$$

see sections 3.3 and 4.2. For such systems an identification of the fast beta transitions with the comparative half-lives corresponding to $logft \leq 4$ allows for the spin and parity assignment of $I^\pi = 1^+$ to the populated levels in daughter odd–odd isobar. The relative GT strength distribution is a measure of a contribution of the $1^+(\pi g_{9/2}^{-1}, \nu g_{7/2})$ configuration in the wave functions of the 1^+ levels.

A dominant role of the even–even core is also manifested in the beta decays of odd–A and odd–odd nuclides. For such nuclei, the multiquasiparticle structures at high excitation energies were found to be strongly populated, see sections 3.4 and 4.5. A particularly interesting aspect of such decay pattern for nuclei close to ^{100}Sn is related to the enhancement of the beta-delayed proton emission, as is discussed in subsections 3.4.1 and 4.5.2.

11

3 Experimental Studies on Beta Decay in the ^{100}Sn region

Most of the decay spectroscopy studies of nuclei in the ^{100}Sn region have been performed at the on–line mass separators at GSI Darmstadt, ISOLDE/CERN Geneva and LISOL Louvain–la–Neuve. The descriptions of these facilities are given in [65], [66, 67], and [68], respectively.

Heavy–ion reactions have been used for the production of neutron–deficient nuclei in the ^{100}Sn region at GSI. Beams of ^{40}Ca and ^{58}Ni at 4 to 5 MeV/u, on enriched ^{50}Cr, ^{58}Ni and ^{60}Ni targets, were usually applied. The results of these experiments were strongly related to the progress in the ion–source technique [69]. The bunched beam release method [70] developed at GSI as well as the laser induced extraction [71, 72, 73] have added chemical selectivity to the mass separated beams. In the best cases, samples containing almost only one radioactive isotope have been collected at the detector stations behind the GSI on–line mass separator.

Mass–separated cadmium beams, produced at ISOLDE with protons or ^{3}He on a molten tin target were also generally free of isobaric contamination of neighbouring elements. However molecular ions of $^{A-23}$Br^{23}Na^{+} were sometimes present in the separated samples of A–isobars [18].

Pioneering decay studies of ligth indium isotopes, like the identification of ^{101}In [74] and the observation of a shift of the β–strength function to higher energies in the ^{104}In decay [75], were performed at the LISOL facility in Louvain–la–Neuve. However, the rates of the most exotic nuclei produced there were limited by the available heavy–ion beams (up to ^{20}Ne). Large target thicknesses and beam intensities (10^{12} pps level) cannot compensate the drop of the cross section. A comparison of the production cross sections for neutron–deficient tin isotopes in the reactions ^{58}Ni + ^{50}Cr (GSI) and ^{20}Ne + ^{92}Mo (LISOL), calculated according to a statistical model of formation and deexcitation of a compound nucleus (HIVAP code [76]), is given in Fig.3.

Typical examples of the performed decay studies and a summary of experimental data on GT-strength available–to–date are given in the following sections.
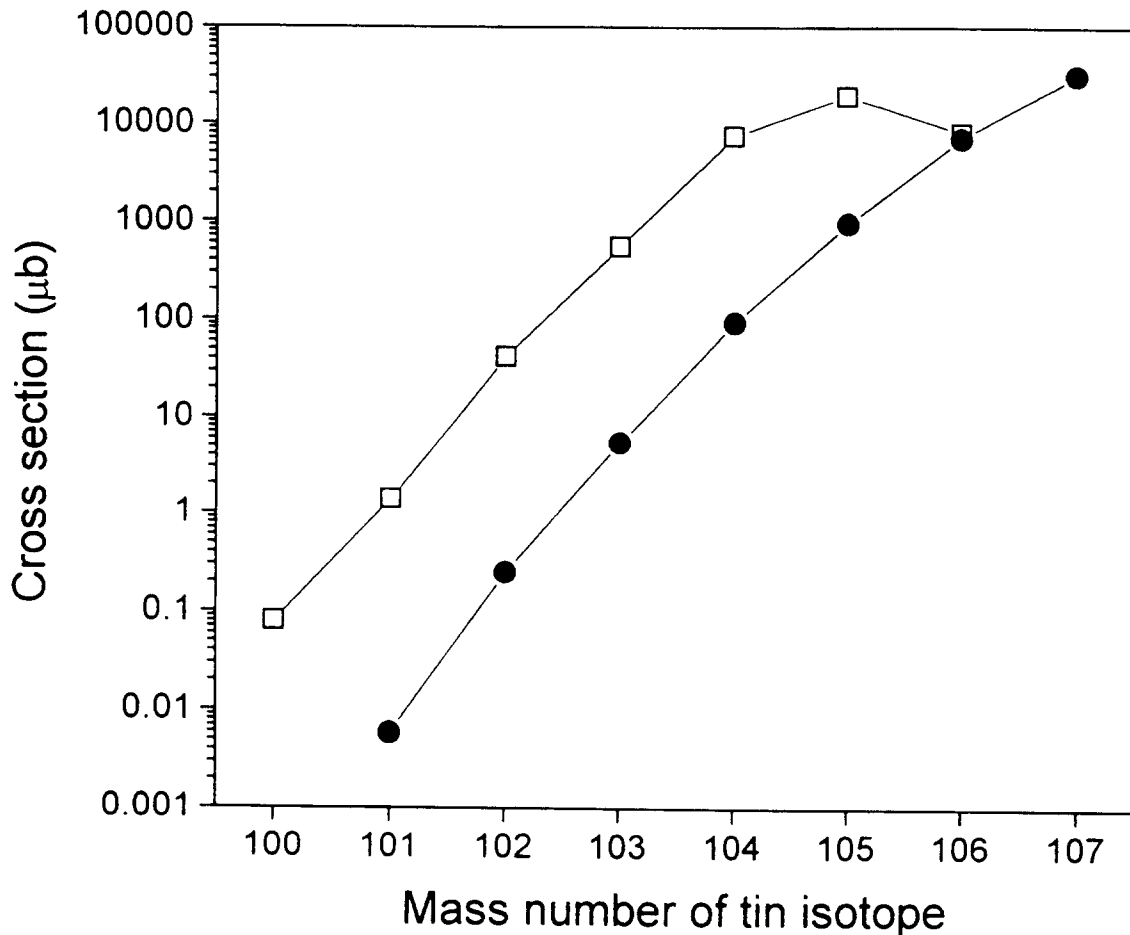
12

Figure 3: Cross sections for production of neutron–deficient tin isotopes in the heavy-ion reactions: ^{58}Ni(5 MeV/u) + ^{50}Cr(3 mg/cm^2) – open squares, and ^{20}Ne(10 MeV/u) + ^{92}Mo(30 mg/cm^2) – solid circles. The data, calculated by using the HIVAP code [76], are averaged over the respective target thickness.

3.1 Experimental Gamow–Teller Transition Strength

The experimental determination of the total GT transition strength $B^{exp}(GT)$ in beta decay corresponds to the conversion of the measured comparative half–lives $f_i t_i$ into $B_i(GT)$ and summing over all observed transitions:

$$B^{exp}(GT) = \sum_i B_i(GT) = \sum_i \frac{3860}{f_i t_i} \quad , \qquad (4)$$

where 3860±18 s is the ratio of the constants appearing in formula (1), see chapter 2.

The determination of $f_i t_i$ requires experimental data both for the calculation of the phase space factor f_i, and the partial half–life t_i. To obtain f_i, information on the atomic number Z and the transition energy E_i is needed:

$$f_i = f(Z, E_i) \quad , \tag{5}$$

see compilations [54, 55]. The transition energy E_i is equal to the difference between the decay energy Q_{EC} and the excitation energy E_i^* of the level in the daughter nucleus populated directly in the beta decay

$$E_i = Q_{EC} - E_i^* \quad . \tag{6}$$

The decay energy Q_{EC} is taken as a mass difference between the parent and daughter nuclides. Measurements of the beta decay half–life $T_{1/2}$ and branching ratios of beta transitions $(I_\beta)_i$ are necessary to get partial half–life values

$$t_i = \frac{T_{1/2}}{(I_\beta)_i} \quad . \tag{7}$$

The accuracy of the experimental Gamow–Teller total strength value $B^{exp}(GT)$ and the strength distribution $B_i(GT)$ depends mostly on the precision of the individual phase space factor f_i and the partial half–life t_i, since both parameters are usually determined less accurate than the constant used in formula (4). The partial half–life t_i is proportional to the measured $T_{1/2}$ and $(I_\beta)_i^{-1}$ values, but the factor f_i is related to the beta transition energy E_i via a polynomial of the second order for EC decay and of approximately fifth order for β^+ decay. Therefore the accuracy of $B^{exp}(GT)$ value is governed by the precision of E_i. Since level energies E_i^* are usually obtained in γ–spectroscopy studies with a precision better than 1 keV, it is the accuracy of the Q_{EC} determination which in most cases defines the error of f_i and of the resulting $B_i(GT)$ and $B^{exp}(GT)$ values.

3.2 Nuclide Masses and Mass Differences

The methods of determining nuclide masses can be divided into two groups: direct measurements with different types of mass spectrometers and indirect measurements employing nuclear reactions and/or decay chains.

In the first group, ions are selected according to their mass and charge state. In principle, precise information on the magnetic rigidity or cyclotron frequency and time–of–flight are sufficient to determine the mass of the transmitted ion. Additionally, new mass values are often obtained relative to known ones usually analysed in the same

14

experiment. Among the most recent applications of such approach (with a possible extention to the ^{100}Sn region) are the experiments employing a Penning trap at the ISOLDE mass separator [77], the programme of using the second cyclotron at GANIL as a spectrometer with a very long flight path [78] and the mass measurements at the storage ring ESR at GSI [79].

However, the data used so far in the analysis of the beta decay of exotic nuclei in the ^{100}Sn region have been obtained mostly with indirect methods. Examples of such measurements are briefly described below. In these experiments performed at the GSI on–line mass separator, the endpoint energy $E_{\beta+}^{max}$ of the positrons emitted in the GT–decay has been determined.

In case of ^{96}Pd [80], the $E_{\beta+}^{max}$ value has been deduced from a comparison of the experimental and theoretical electron capture to positron emission probability ratio, while for ^{102}Cd decay [81] the energy spectrum of positrons was measured. For ^{104}Sn, both types of measurements were performed [82, 83].

For the production of ^{96}Pd and the study of its decay, a fusion–evaporation reaction ^{40}Ca(4.2 MeV/u) + ^{60}Ni(3.2 mg/cm^2) was used. Recoil products were stopped in a 27 mg/cm^2 carbon catcher inside the ion source of FEBIAD–E type [65], ionized and after extraction accelerated to 50 keV. Mass separation was done in a magnetic field of 0.2 T. Radioactive samples were collected on the moveable tape and transported period-ically to the counting position inside an aluminium annihilator. The annihilator shield allows to stop emitted positrons close to the source, so that the detection solid angles for the annihilation radiation and beta–delayed γ–rays were approximately identical. The γ–singles spectra and γ–γ coincidence data allowed to construct the decay scheme. It was also possible to separate the observed total beta intensity of $I_\beta = 39\%$ per decay populating the excited state at 1275 keV in the daughter ^{96}Rh isotope into two com-ponents. The part related to the electron capture process was measured to be $I_{EC} = 29\%$ while the remaining $I_{\beta+} = 10\%$ was associated with the positron emission. From the $I_{\beta+}/(I_{EC} + I_{\beta+})$ ratio the β^+–endpoint energy was deduced to be 1149±50 keV, corresponding to $Q_{EC} = 3446\pm50$ keV. An account for the systematic errors, mostly related to the possible angular–correlation effect and its influence on the observed γ–γ coincidence intensities increased the estimated Q_{EC} error. The decay energy of ^{96}Pd was finally reported as $Q_{EC} = 3450\pm150$ keV [80].

15

This method is only applicable in a limited energy range of the emitted positrons. Closer to ^{100}Sn the β^+–endpoint energies are above $2\,\text{MeV}$,and the positron emission starts to dominate the decay process. The $I_{\beta+}/(I_{EC} + I_{\beta+})$ depends only weakly on the $E_{\beta+}^{max}$ value, resulting in the large uncertainties in determination of the decay energy, see e.g. the measurement on the ^{104}Sn decay [82].

More precise data can be obtained with the direct measurement of the positron energy spectra. One component of the usually complex beta spectrum could be selected with a gating condition on the characteristic γ–line. In the summation–free β^+–endpoint spectrometer used at GSI on–line mass separator [84] the summing of the positron energy with the annihilation radiation was prevented by detecting both $511\,\text{keV}$ annihilation quanta in the opposite segments of a BGO–ring detector surrounding the positron detector ($11\,\text{mm}$ thick Si). Such measurements [81] were performed for ^{102}Cd activity produced in a ^{58}Ni($5\,\text{MeV/u}$) + ^{50}Cr($3\,\text{mg/cm}^2$) reaction and separated with similar technique as for ^{96}Pd case. The β^+–endpoint energy of the transition populating $I^\pi = 1^+$ level at $481\,\text{keV}$ in ^{102}Ag was determined with a precision of $8\,\text{keV}$, resulting in Q_{EC} of $2587\pm8\,\text{keV}$. In the same experiment the decay energy value of ^{104}Sn was obtained more accurately than with the $I_{\beta+}/(I_{EC} + I_{\beta+})$ ratio method giving a final value of $4515\pm60\,\text{keV}$. This result, together with the measured energies of alpha particles [85, 86, 87] and protons [88, 89] emitted from the ground–states of heavier nuclei was used for the determination of masses [82, 83] of ^{109}I and ^{113}Cs – the latter nuclei beyond the proton drip–line!

3.3   Decay of Even–Even Nuclei and High Resolution Spectroscopy

There are fourteen even–even isotopes in the section of the chart of nuclides delimited by the beta stability line, the chain of $N = 50$ isotones and the chain of $Z = 50$ tin isotopes, see Fig.4. Beta decays of twelve of them, namely ^{94}Ru [90], ^{96}Pd [80], ^{98}Pd [91], ^{100}Pd [91, 92], ^{98}Cd [18, 93], ^{100}Cd [93], ^{102}Cd [81], ^{104}Cd [94], ^{104}Sn [82, 95, 96], ^{106}Sn [95], ^{108}Sn [95] and ^{110}Sn [97] have already been studied. One of the remaining two, ^{102}Sn, has been identified for the first time with $\Delta E, E - TOF$ technique in the experiment at LISE3 fragment separator at GANIL among the products of the reaction ^{112}Sn ($58\,\text{MeV/u}$) + ^{nat}Ni ($75\,\text{mg/cm}^2$) [98]. However, in this experiment, several
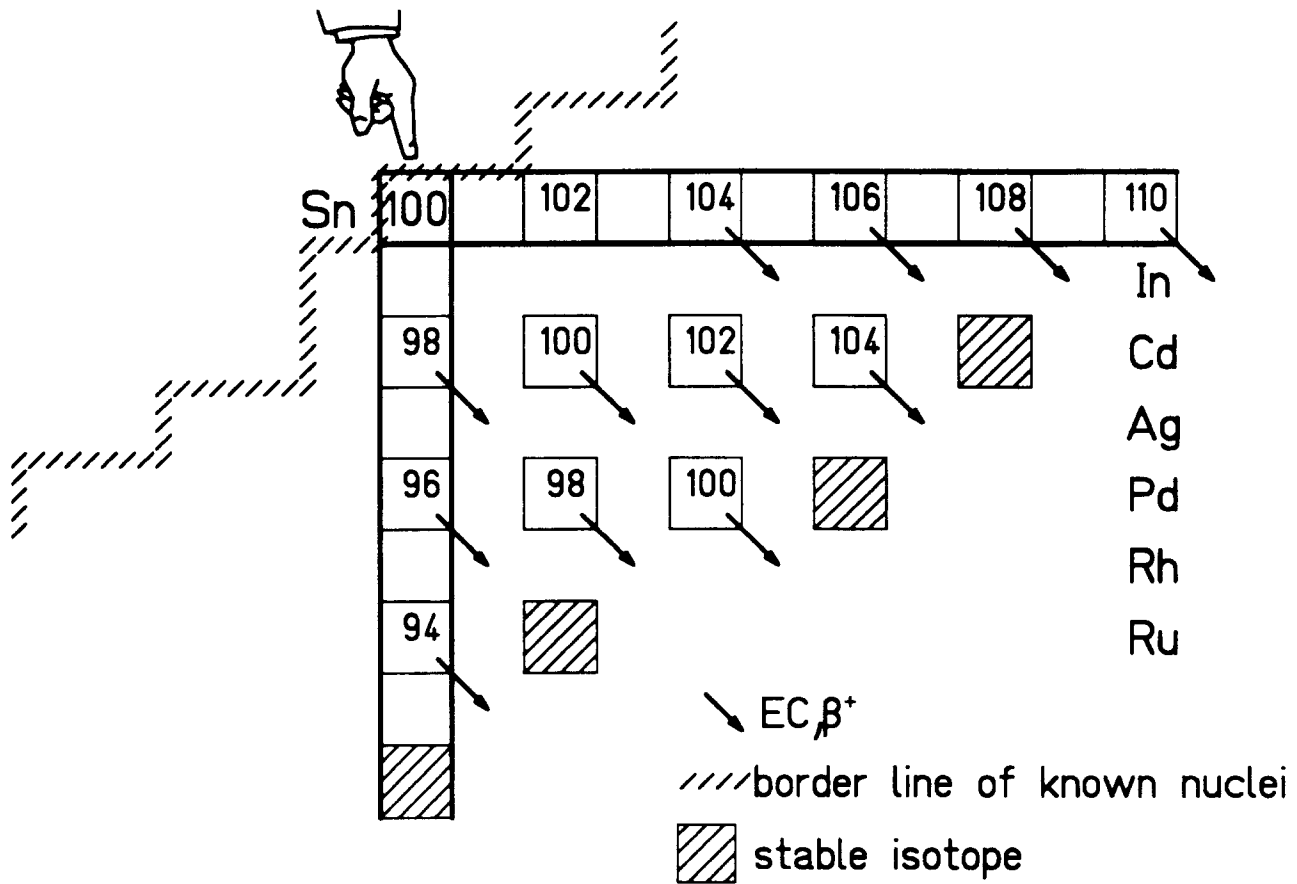
Figure 4: Section of the chart of nuclei near ^{100}Sn. The studied decays of even–even nuclides are marked by the arrows.

tens of observed ^{102}Sn events were not sufficient to determine the half–life or other beta decay properties.

After many experimental attempts to approach ^{100}Sn [6, 98, 99] seven events assigned to this nucleus have recently been reported [1] as a result of 12 days counting with the use of the ^{124}Xe beam (1.1 GeV/u) on a ^{9}Be (6 g/cm^2) target and the fragment separator FRS at GSI Darmstadt. The first experimental estimation of the half–life $0.4\,\text{s} < T_{1/2} < 1.3\,\text{s}$ based on four events correlated with β–decay has been given [100]. Also the half–life of ^{102}Sn has been determined as $3.4\pm0.7\,\text{s}$.
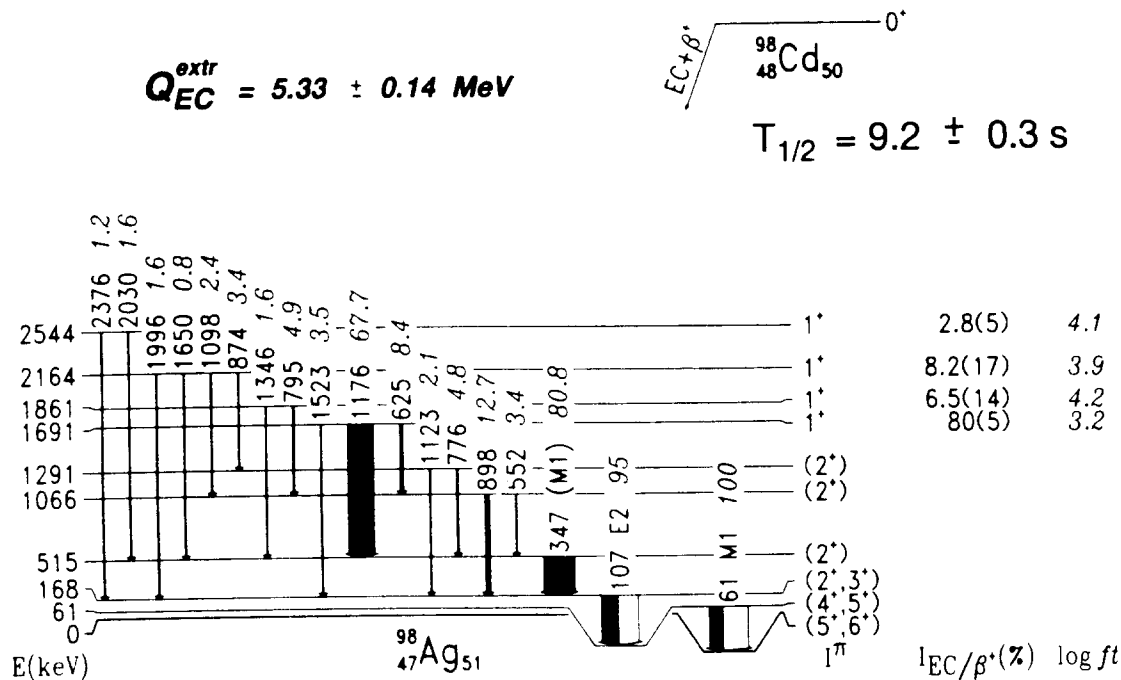
$Q_{EC}^{extr} = 5.33 \pm 0.14$ MeV

$^{98}_{48}Cd_{50}$ ——— 0⁺ ... EC+β⁺

$T_{1/2} = 9.2 \pm 0.3$ s

2544 ————————————————————— 1⁺   2.8(5)   4.1

2164 ————————————————————— 1⁺   8.2(17)   3.9

1861 ————————————————————— 1⁺   6.5(14)   4.2

1691 ————————————————————— 1⁺   80(5)   3.2

1291 ————————————————————— (2⁺)

1066 ————————————————————— (2⁺)

515 ————————————————————— (2⁺)

168 ————————————————————— (2⁺,3⁺)

61 ————————————————————— (4⁺,5⁺)

0 ————————————————————— (5⁺,6⁺)

E(keV) $^{98}_{47}Ag_{51}$ I$^\pi$ I$_{EC/\beta^+}$(%)   log ft

(transition energies in keV with intensities in italics: 2376 1.2, 2030 1.6, 1996 1.6, 1650 0.8, 1098 2.4, 874 3.4, 1346 1.6, 795 4.9, 1523 3.5, 1176 67.7, 625 8.4, 1123 2.1, 776 4.8, 898 12.7, 552 3.4, 347 (M1) 80.8, 107 E2 95, 61 M1 100)

Figure 5: The decay scheme of ^{98}Cd (from [18]). The transitions in ^{98}Ag are marked by their γ–ray energies in keV and total transitions intensities per hundred decays (given in italics). The multipolarities M1 for the 61 keV line and E2 for the 107 keV transition have been experimentally determined while M1 has been adopted for the 347 keV line.

An order of magitude higher rate was achieved in the independent and almost simultaneous experiment at GANIL Caen [2, 3]. Twenty four ^{100}Sn ions were identified during 44 hours among the products of the ^{112}Sn beam (63 MeV/u) on a ^{nat}Ni target (144 mg/cm²) fragmentation–like reaction. There are already methods developped [2, 3] to improve the rate of this exotic nucleus at GANIL by a factor of five, which could make its decay study realistic in the near future.

As seen in Fig.4, ^{98}Cd is the closest even–even nucleus to ^{100}Sn, of which the decay has been studied [18]. As an example of the investigations performed with the high resolution spectroscopy methods, the data on this decay are briefly presented below. The decay scheme given in Fig.5 is based on the results of several measurements at the

ISOLDE on-line mass-separator [93, 18] at CERN. Three arrangements of detectors were used at the measuring point of the tape system transporting periodically the collected mass–separated samples. High resolution Ge detectors were used to measure X– and γ–rays in the energy range from $10\,\mathrm{keV}$ to $6\,\mathrm{MeV}$.

To determine the multipolarity of low energy gamma–transitions, conversion electrons were measured by means of a mini–orange spectrometer [101]. Singles and coincidence measurements were performed. A typical experiment lasted about ten 8–hour shifts, with approximately a 50% duty cycle.

Prior to our studies [93, 18] no information on the decay of ^{98}Cd was available except a rough estimation of the half–life $\sim 8\,\mathrm{s}$ derived from a weak, short–lived component in the complex beta spectrum of mass–separated $A = 98$ samples [102]. Presently, the decay scheme of ^{98}Cd contains nine levels in ^{98}Ag and accounts for all but one of the identified 19 γ–transitions, as well as for all measured coincidence relations. There are four levels directly fed by the EC/β^+ transitions with comparative half–lives corresponding to $log(ft)_i \leq 4.2$. This indicates an allowed character of the observed beta transitions and consequently the spin and parity assignment of $I^\pi = 1^+$, see chapter 2.

Each derived $f_i t_i$ value was converted into $B_i(GT)$ strength, see formula (4), and the $B(GT)$ distribution obtained this way is given in Fig.6 together with experimental sensitivity limit for the GT strength detection related to the limit of the observable γ–line intensity.

In fact, the gamma intensity balance does not take into account the feeding of levels in ^{98}Ag by the undetected weak γ–transitions. There are two main questions related to this problem. The first one concerns $I^\pi = 1^+$ levels reported as directly populated by beta–transitions. It migth be argued that the reported beta branching $(I_\beta)_i$, used for the calculation of the $f_i t_i$ value and following a $I^\pi = 1^+$ assignment, is too high because the $(I_\beta)_i$ deduced from the intensity balance could be the sum of real beta–feeding and undetected γ–intensity. Of course, this refers to the hypotetetical γ–line feeding considered $I^\pi = 1^+$ level and presumably non–encountered due to the detection limit. However, such undetected γ–transitions can only originate from 1^+ levels (i.e. the only states fed directly by beta transitions) above the discussed one. But as observed in odd–odd nuclei near ^{100}Sn, the transitions between 1^+ states have very low probability.
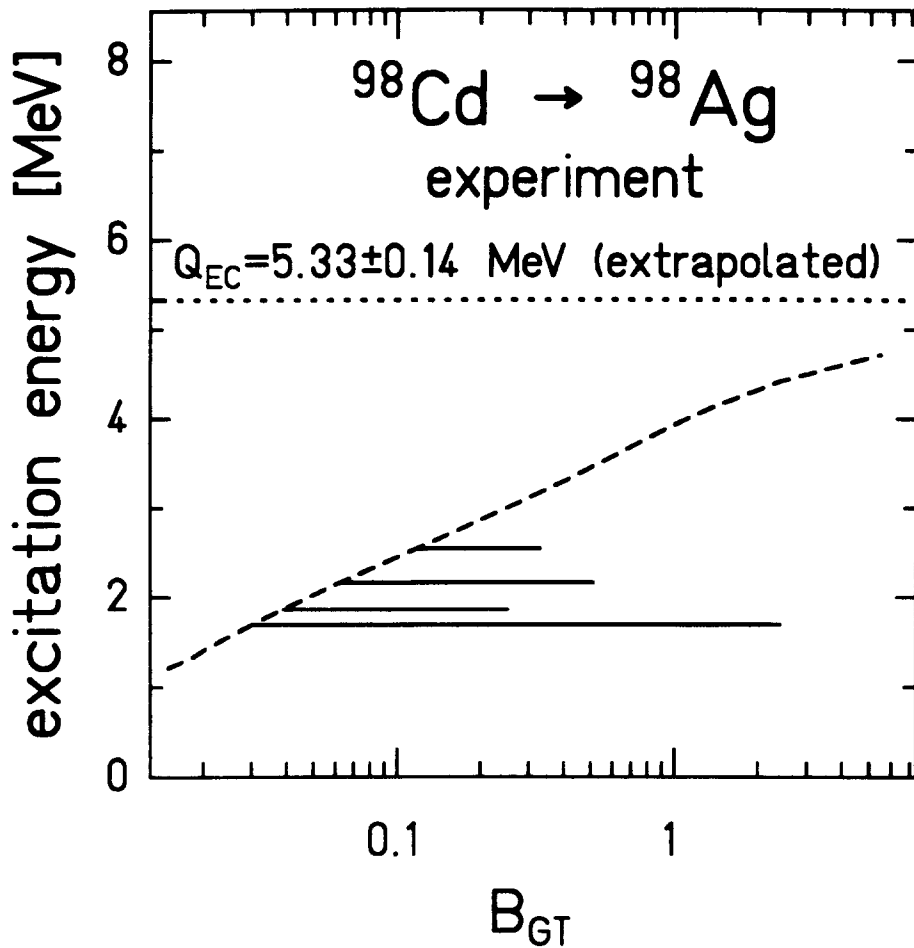
Figure 6: GT–strength distribution derived for the decay of ^{98}Cd. The dashed line indicates the experimental sensitivity limit. The Q_{EC} value of 5.33±0.14 MeV has been estimated via the extrapolation of decay energies measured for even N=50 isotones and even cadmium isotopes, see [18].

The main deexcitations of such 1^+ states populate the low–lying $I^\pi = 2^+$ states, and sometimes $I^\pi = 3^+$ states. The assumption on γ–feeding from an unknown 1^+ state to the discussed 1^+ level would require a presence of a stronger transition to the known 2^+ state, which would lead first of all to the identification of a new $I^\pi = 1^+$ state. Imaginable but undetected decay to the lower 1^+ state would be much weaker then such transition to the known $I^\pi = 2^+$ level. Therefore weak undetected γ–lines
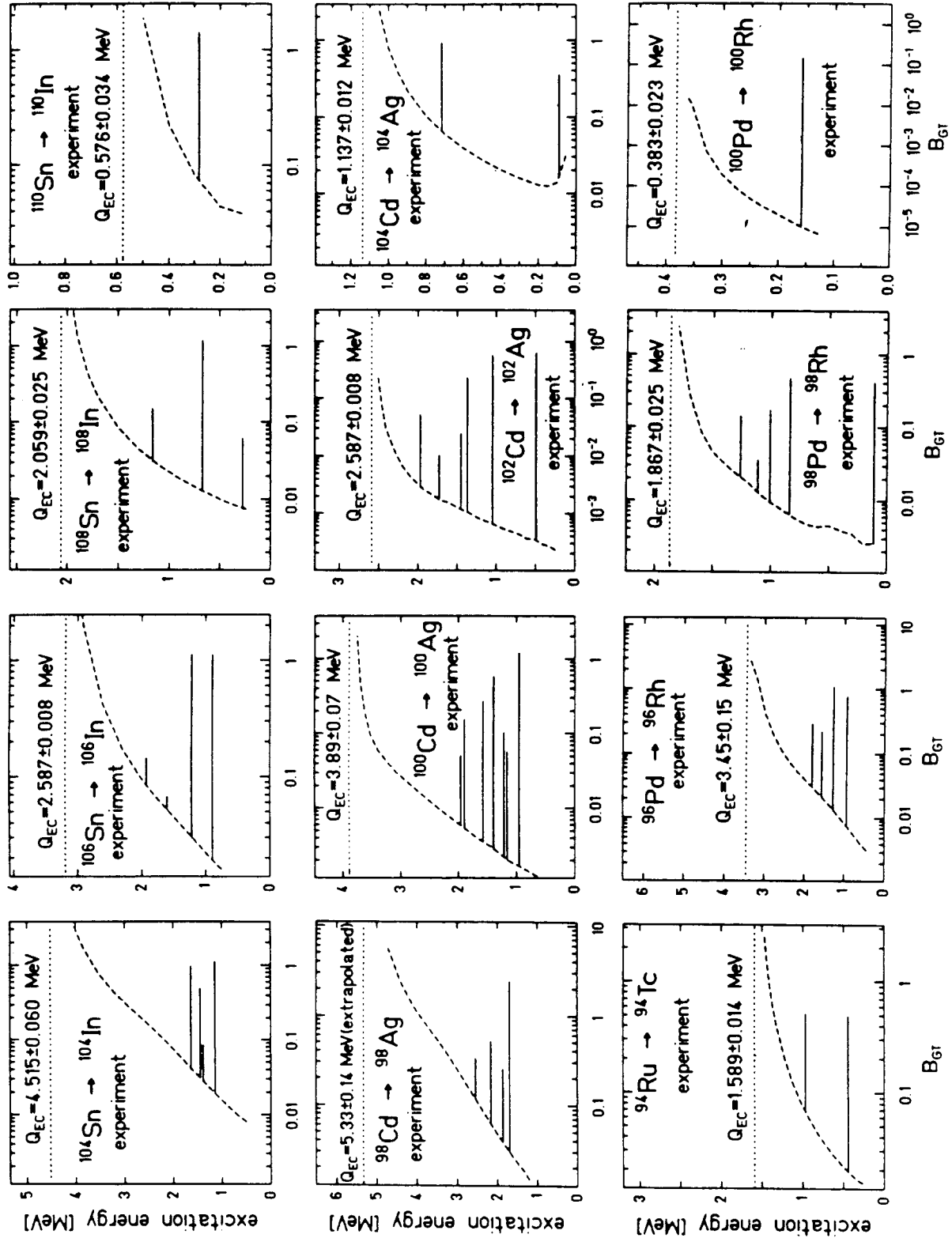
20

Figure 7: GT–strength distribution observed in the decays of even–even nuclides in the ^{100}Sn region (from [6]). Dashed lines indicate experimental sensitivity limits for the GT–strength detection (see text).

cannot affect substantially the reported beta branching ratios and do not change the $I^\pi = 1^+$ assignments.

However, undetected γ-transitions may in a second way have a quite large influence on the GT strength distribution. Even a relatively low beta branching ratio to a 1^+ level at an excitation energy E_{1+} close to the upper energy limit set by Q_{EC} value, followed by presumably undetected γ-lines to the $I^\pi = 2^+$ levels, may correspond to a quite large $B(GT)$ value (see sensitivity limits given in Fig.6 and Fig.7). It is obvious that a reliable estimation of the strength "hidden" under the sensitivity limit and located above the decay energy window is crucial for the discussion of the "missing strength" problem.

The summary of the experimental information available–to–date on the GT strength in the decays of twelve even–even nuclei in the ^{100}Sn region is given in Fig.7. There are a few $0^+ \rightarrow 1^+$ transitions identified in each decay, with the exception of ^{100}Pd and ^{110}Sn. For the latter two cases, the observations of only one 1^+ state in the daughter ^{100}Rh and ^{110}In nuclei are apparently connected with the low Q_{EC} values, about 0.4 MeV and 0.6 MeV, respectively. Other 1^+ levels are at too high excitation energy to be populated in the beta decay.

The seven 1^+ states identified in ^{100}Ag reflect the good experimental conditions during the spectroscopic studies of the ^{100}Cd decay at ISOLDE.A production rate up to 70 000 atoms/s and the chemically pure cadmium beams allowed the detection of gamma transitions down to the intensity limit of about 0.1% per decay [93].

3.4 Decays of 'Non Even–Even' Nuclides

The dominating beta transition in the decay of even–even nuclei in the ^{100}Sn region, i.e. the $\pi g_{9/2} \rightarrow \nu g_{7/2}$ GT-transformation, governs also the decay of the neighbouring odd–A and odd–odd nuclides, see Fig.2. However, the ground-state spin I_i of the considered 'non even–even' parent nuclei usually differs from zero. According to the GT–selection rules (section 2.1), the final levels having spins $I_f = I_i$, $I_i \pm 1$ are expected to be populated. The parent nuclides for the decays disscused below are indicated in Fig.8.
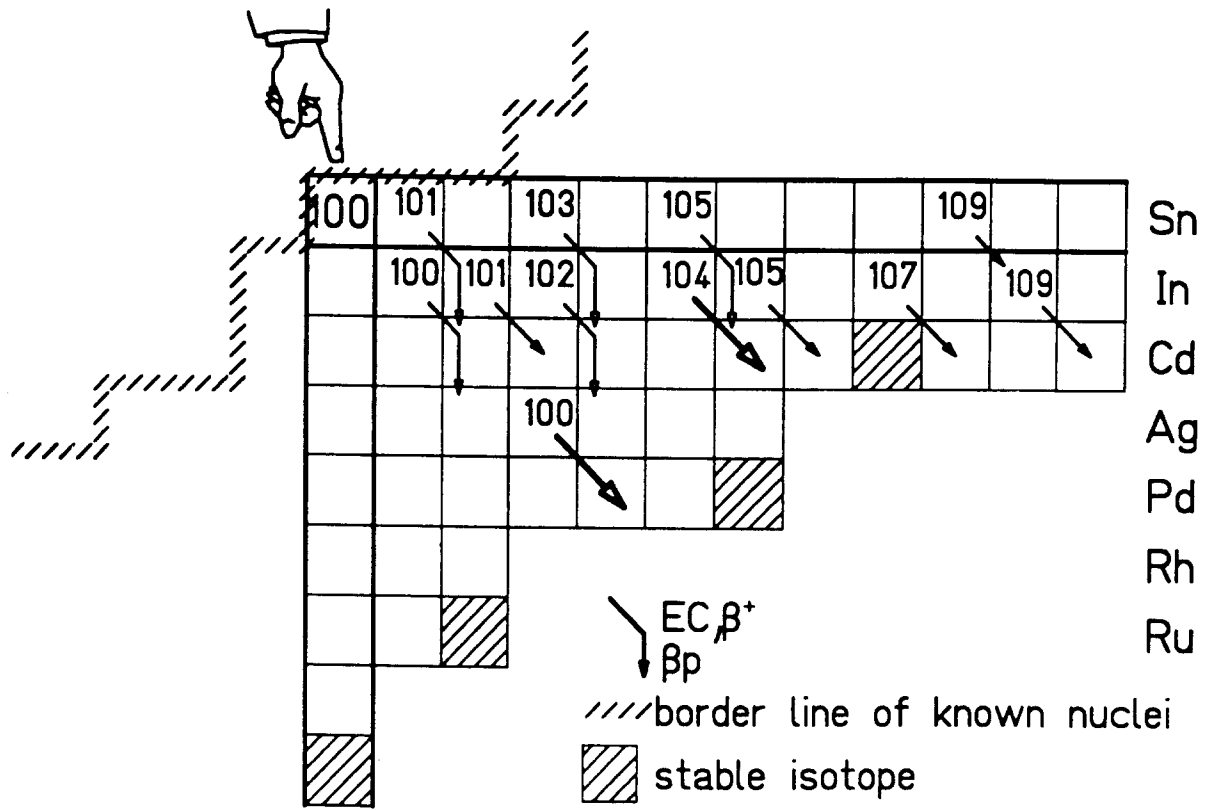
Figure 8: Decays of the 'non even–even' nuclides in the ^{100}Sn region ($N \geq 50$, $Z \leq 50$) discussed in the text. There are five beta–delayed proton precursors indicated with the broken arrows. The decays of two odd–odd nuclides, $^{100}_{47}$Ag$_{53}$ and $^{104}_{49}$In$_{55}$, studied with the Total Absorption Gamma Spectrometer (TAGS) are marked with bold solid arrows.

Spin and parity of the ground–state of the even–Z, odd–N system is determined by an odd neutron coupled to $I^{\pi} = 0^{+}$ of the even–even core. For the nuclei with a few neutrons above the closed neutron shell $N = 50$ the last odd neutron should be in the $d_{5/2}$ state, see Fig.2. It will play only a role of a spectator in the $\pi g_{9/2} \rightarrow \nu g_{7/2}$ GT–transformation. This transformation occurs within the even–even core and is thus analogous to the $0^{+} \rightarrow 1^{+}$ decay of the neighbouring even–even nuclides. It leads to three–quasiparticle ($3qp$) states in the odd–Z, even–N daughter at excitation energies exceeding 2Δ. The pairing gap parameter can be roughly estimated from the relation $\Delta \approx 12/\sqrt{A}$ MeV.

In the case of an odd–odd parent, the GT–decay should also occur in the even–even core, leading to four-quasiparticle ($4qp$) configurations at about 4Δ in the even–even daughter. However, a possibility of GT transitions to two–quasiparticle ($2qp$) states, corresponding to a transformation of the odd proton, cannot be neglected.

3.4.1 Beta–Delayed Protons

General considerations on the decays of 'non even–even' nuclides can be illustrated with the $^{101}Sn \rightarrow ^{101}$In case. The GT–transition can be expressed as

$$5/2^+ \{0^+(\text{core}) \otimes 5/2^+ \nu d_{5/2}\} \rightarrow I_f\{1^+(\pi g_{9/2}^{-1}, \nu g_{7/2}) \otimes 5/2^+ \nu d_{5/2}\} \ .$$

The energy of such a $3qp$ final state in $^{101}_{49}$In$_{52}$ is estimated to be above $2.4\,\text{MeV}$ with respect to the $9/2^+\{9/2^+ \pi g_{9/2}^{-1} \otimes 0^+ \nu d_{5/2}^2\}$ ground-state. This is essential for beta–delayed proton emission.

The proton separation energy S_p in the daughter ^{101}In is about $1.4\pm0.3\,\text{MeV}$ [104], i.e. below the expected excitation energy of the levels fed in the GT–decay of ^{101}Sn. Since the decay energy of ^{101}Sn is estimated to be $8.9\pm0.6\,\text{MeV}$ [104], the energy window for the proton emission from the excited states of ^{101}In is quite large, $Q_{EC} - S_p \approx 7.5\,\text{MeV}$. This makes favourable conditions for the protons competing with γ–deexcitation mode. In the subsequent ^{101}In decay this is not the case as the $Q_{EC} - S_p$ value is only $2.9\,\text{MeV}$. Therefore, the proton detection provides a relative enhancement of ^{101}Sn activity against the isobaric contamination of ^{101}In in a mass separator based experiment. In addition, the detection of protons does not suffer from laboratory background, the latter representing a major problem for gamma counting during a search for weak activities.

For several neutron-deficient nuclides in the region of ^{100}Sn, measurements of the proton energy spectra allowed for the identification of new isotopes and yielded the first information on their decay properties. The studies of odd–mass isotopes like ^{103}Sn and ^{105}Sn [105], and most recently of the closest neighbours of ^{100}Sn namely ^{101}Sn [103] and ^{100}In [106], are the best examples. For ^{101}Sn, the half-life value of $3\pm1\,$s was so far derived only from the time structure of beta–delayed proton radiation [103]. For ^{100}In the value of $T_{1/2} = 6.1\pm0.9\,$s obtained from the proton spectra measured at the on–line mass separator [106] was confirmed with the study of the time distribution of beta events ($T_{1/2} = 7.8\pm0.8\,$s) following the implantation of ^{100}In ions into thick Si–counter during the projectile–fragment separator FRS experiment [100].

Such an experimental half–life determination already allows for the first test of the theoretically predicted GT–strength properties, see subsection 4.5.2. Also from the measured proton energy spectra an estimation of the decay energy could be derived supporting the model extrapolations (see e.g. the discussion in [106]).

3.4.2 Broad GT–Strength Distributions and $4\pi-$ Counting

While limited data were obtained so far on the decay properties of such exotic nuclei as ^{101}Sn and ^{100}In, more information on the decay schemes have been reported
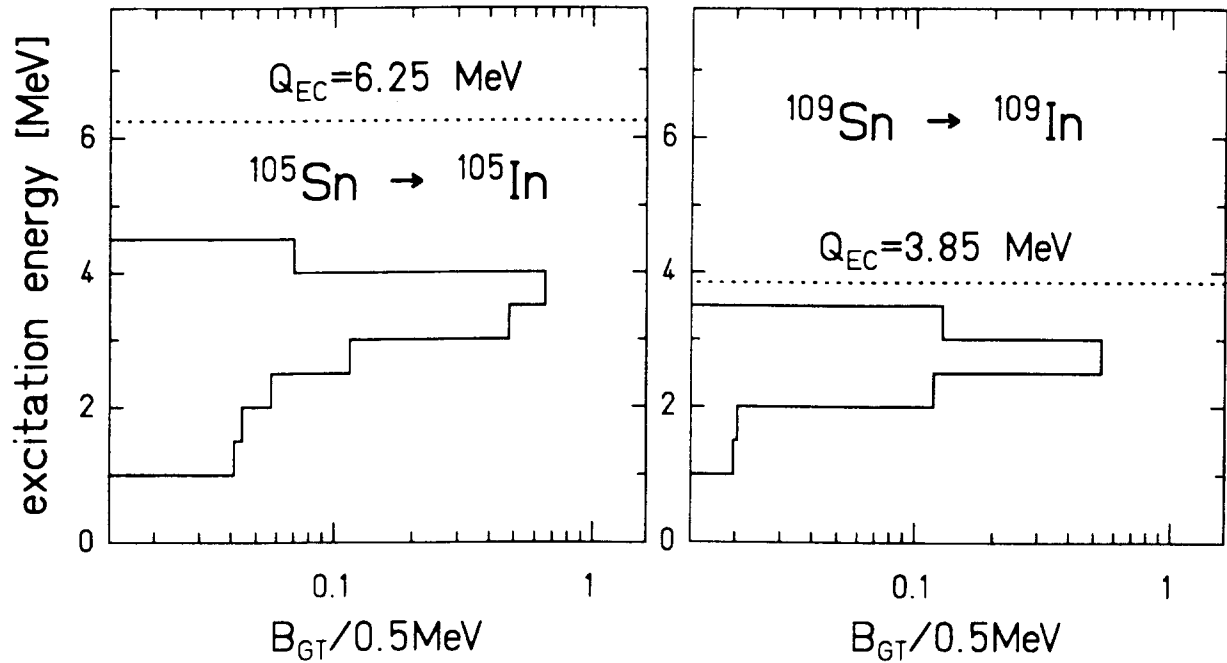
Figure 9: The GT–strength distributions derived for the ^{105}Sn [107] and ^{109}Sn [108] decays from the experimental data obtained with high resolution but low efficiency spectroscopy methods.

for other 'non even–even' nuclides in the ^{100}Sn region – expected to reveal similar decay properties. GT–strength distributions observed for heavier tin isotopes like ^{105}Sn [107] and ^{109}Sn [108] have broad resonant structures with maxima at about 3 to 4 MeV excitation energy, see Fig.8. The total summed strengths $B^{exp}(GT)$ are lower by a factor of about 2 then the values found for neighbouring even–even isotopes, see Table 2. Such strength reduction for the odd–A tin isotopes compared to the even ones is in discrepancy with the theoretical expectations, see the calculations of Towner [12] or the recent predictions of Borzow et al [16, 21].

Table 2: Total GT–strength values measured for ^{105}Sn and ^{109}Sn compared to the ones found for the neighbouring isotopes of tin. The respective decay energies are also given.

Isotope	^{104}Sn	^{105}Sn	^{106}Sn	^{108}Sn	^{109}Sn	^{110}Sn
$B^{exp}(GT)$	$2.6^{+0.4}_{-0.3}$	≥ 1.46	$2.4^{+0.3}_{-0.3}$	$1.4^{+0.1}_{-0.1}$	0.82	$1.4^{+0.5}_{-0.3}$
Q_{EC}[MeV]	$4.515\pm.06$	$6.25\pm.08$	$3.18\pm.05$	$2.059\pm.025$	$3.85\pm.01$	$0.638\pm.019$

The decay energies of ^{105}Sn and ^{109}Sn are larger than those of neighbouring even isotopes, see Table 2. In particular for ^{105}Sn this should compensate the shift of the populated levels towards higher energies. These *3qp* states should be within the decay energy window and hence the total GT–strength value should be similar to the numbers obtained for neighbouring ^{104}Sn and ^{106}Sn. However, there are purely experimental reasons for missing part of the strength in the studies performed on odd–mass tin decays. The states populated in the respective indium isotopes are in the regions of high level density. This means a spread of the GT–strength over many levels (see also calculations of Brown – chapter 4) followed by γ–deexcitation with very small individual intensity per decay. High resolution but low efficiency gamma spectroscopy is not an appropriate tool to investigate such decay process. The detection of weak γ–lines originating from the regions of high level density and leading to discrete states at lower excitation energies is below the sensitivity of such a method. The beta branching ratios deduced from the apparent intensity balance for low-lying levels are in reality summed beta– plus unobserved (but substantial) gamma–feedings. This results in a shift in the derived strength distribution towards lower energies. Due to the energy dependence of the phase space factor f this causes also an artificial reduction of the total strength.

The interpretation of the beta transitions seen in the decays of odd–Z, even–N nuclei in the ^{100}Sn region, such as $^{101}_{49}$In$_{52}$, should be similar to the one discussed for odd–tin isotopes. An odd–proton on the $g_{9/2}$ orbital defining the ground–state spin and parity $I^{\pi} = 9/2^{+}$ should be transformed into $g_{7/2}$ neutron in $^{101}_{48}$Cd$_{53}$. For the latter nucleus, the final configuration written with respect to the $^{90}_{40}$Zr$_{50}$ core as $7/2^{+} \{\pi g^{8}_{9/2} \otimes \nu d^{2}_{5/2} \otimes \nu g_{7/2}\}$ corresponds to the excited state above the $5/2^{+} \{\pi g^{8}_{9/2} \otimes \nu d^{3}_{5/2}\}$ ground state. The decay of ^{101}In ($T_{1/2} = 16 \pm 3$ s) has been identified a few years ago at the LISOL on–line mass–separator facility at Louvain–la–Neuve [74]. Later on, at GSI two (252 keV and 892 keV) out of four reported [74] γ–transitions were confirmed as the ones following beta decay of this isotope in coincidence with each other. However, such partial information is by far not enough to discuss GT–strength properties. More data are available for ^{105}In [109], ^{107}In [110] and ^{109}In [108] decays, see Fig.10, where the structures at higher excitation energies were found to be primarily populated, in addition to the $7/2^{+}$ excited states at 131 keV, 205 keV and 203 keV in ^{105}Cd, ^{107}Cd and ^{109}Cd, respectively.

These structures can be explained as the ones following even–even core decay, with the unpaired proton in the $g_{9/2}$ orbital remaining as a spectator. Such decay process could be described as EC/β^{+} transitions to the *3qp* states in odd–A cadmium daughters;

$$[0^{+}(core) \otimes 9/2^{+}(\pi g^{1}_{9/2})] \rightarrow [1^{+}(\pi g^{-1}_{9/2}, \nu g_{7/2}) \otimes 9/2^{+}(\pi g^{1}_{9/2})],$$

where *core* denotes here the even–even part of the decaying odd–A nuclide.

Experimental ratios of the beta strength for the two possible decay patterns (g. s.→*3qp* and g. s.→*1qp*) are about 40:1 [109], 37:1 [110] and 11:1 [108] for the ^{105}In, ^{107}In and ^{109}In decays, respectively, showing already the dominant role of even–even core decay, in particular for the decays with larger Q_{EC} windows. The planned investigations on indium decays [8], to be performed with the total absorption gamma spectrometer TAGS, will most probably increase these numbers while finding the branchings to the high–lying states, missed in high resolution, but low efficiency gamma counting.

An even larger difference between the strengths values characterizing the two basic decay paths was found for the decay of odd–odd isotope ^{104}In, see Fig.11. The measured strength ratio is 600:1. GT–decay of the even–even core forms there the *4qp* structure in ^{104}Cd at about 5 to 6 MeV with a "Gamow–Teller pair" $(\pi g^{-1}_{9/2}, \nu g_{7/2})$ coupled to
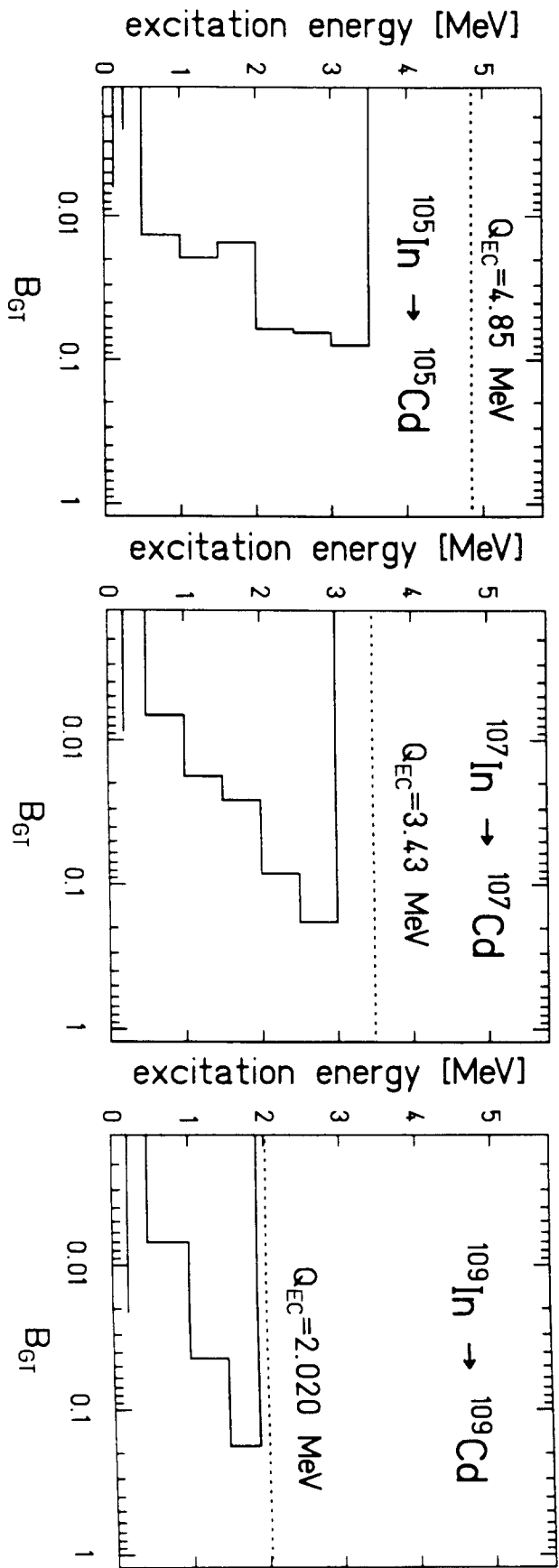
Figure 10: The GT strength distributions reported for the decays of odd-even isotopes of [105]In [109], [107]In [110] and [109]In [108], respectively. The B_{GT} values displayed as a histogram represent a sum over 0.5 MeV excitation energy interval.

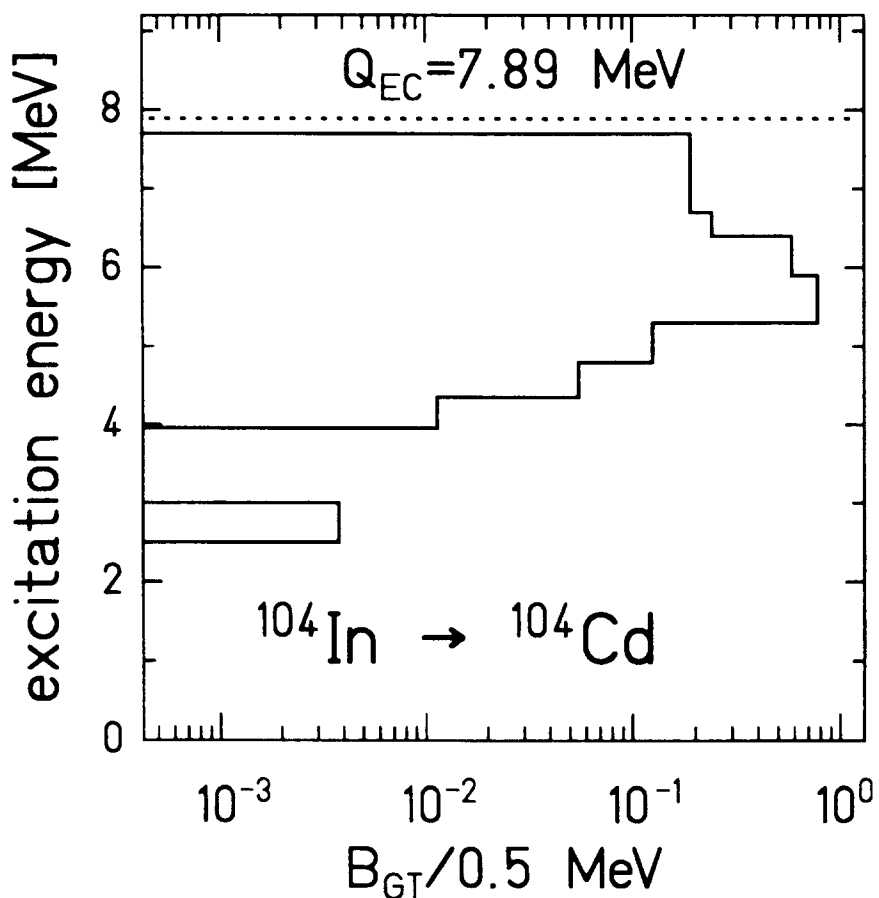Figure 11: The GT–strength distribution determined with the Total Absorption Gamma Spectrometer for the decay of [104]In [6,111].

$I^{\pi} = 1^{+}$ and two odd particles – a $g_{9/2}$ proton and a $d_{5/2}$ or $g_{7/2}$ neutron. A two–neutron quasiparticle state $(\nu d_{5/2}, \nu g_{7/2})$ at about 2 to 3 MeV should also be populated via the direct transformation of the $g_{9/2}$ proton into the $g_{7/2}$ neutron. The data presented in Fig.11 were obtained in the first experiment employing the total absorption gamma spectrometer TAGS [111, 6] for decay studies in the [100]Sn region.

TAGS is a suitable tool to investigate the decays populating states at high level density regions and characterized by the high multiplicity of subsequent gamma decay. The energy released in the gamma deexcitation cascade is summed up in the NaI(Tl) crystal surrounding the radioactive sample, see Fig.12. After a non–trivial calibration and deconvolution of the measured spectra, the true β^{+}/EC feeding pattern should
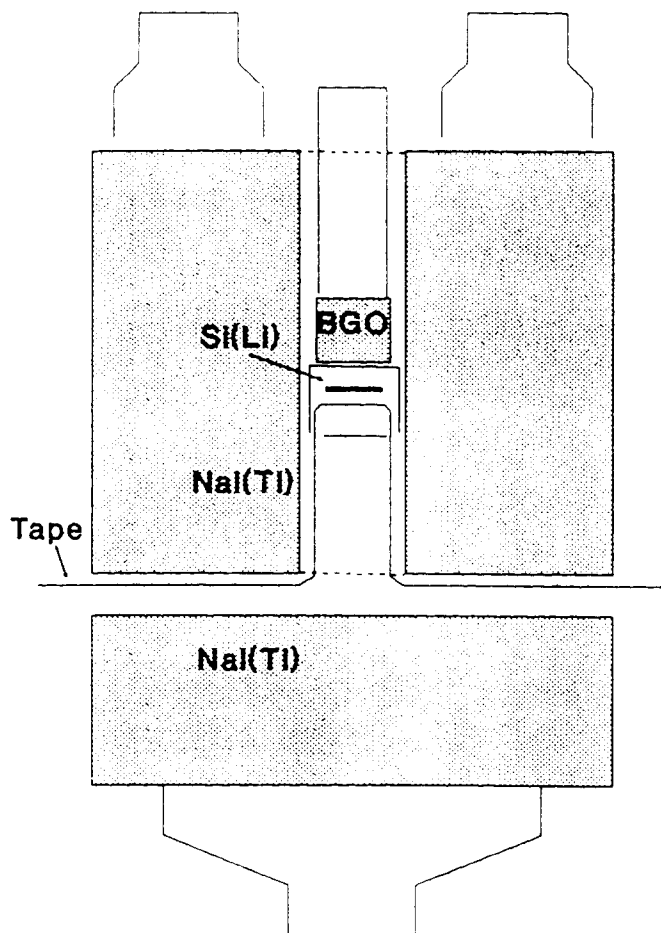
Figure 12: The schematic view of the Total Absorption Gamma Spectrometer (TAGS) constructed at the St. Petersburg Nuclear Physics Institute and used at the GSI on–line mass separator for the decay studies of odd–odd nuclides in the ^{100}Sn region [111,112].

be derived. This can be converted into a realistic GT–strength distribution. So far the decays of $^{104}_{49}$In$_{55}$ (Fig.11) and $^{100}_{47}$Ag$_{53}$ (Fig.13) were studied with this method [111, 106, 112].

Measurements of the average $\beta^+/(EC+\beta^+)$ ratio for ^{104}In [106] with an annihilator technique, see section 3.2, could be used as an independent proof of the TAGS results. The numbers obtained for the ^{104}In decay with these two techniques are in a very good agreement, 0.47±0.03 and 0.45±0.01 with TAGS and the annihilator, respectively. Similar measurements were performed for the ^{102}In decay, however the TAGS data are somewhat preliminary due to the low rate of ^{102}In and problems with the linearity of the energy calibration [106]. A GT–strength distribution cannot be presented yet for this decay. Nevertheless the average $\beta^+/(EC+\beta^+)$ ratios were derived and amount to 0.75±0.05 (TAGS) and 0.72±0.07 (annihilator). These results are indicating again

a quite similar decay pattern as for ^{104}In, but with the decay energy Q_{EC} and the beta–transition energies around 1 MeV higher.
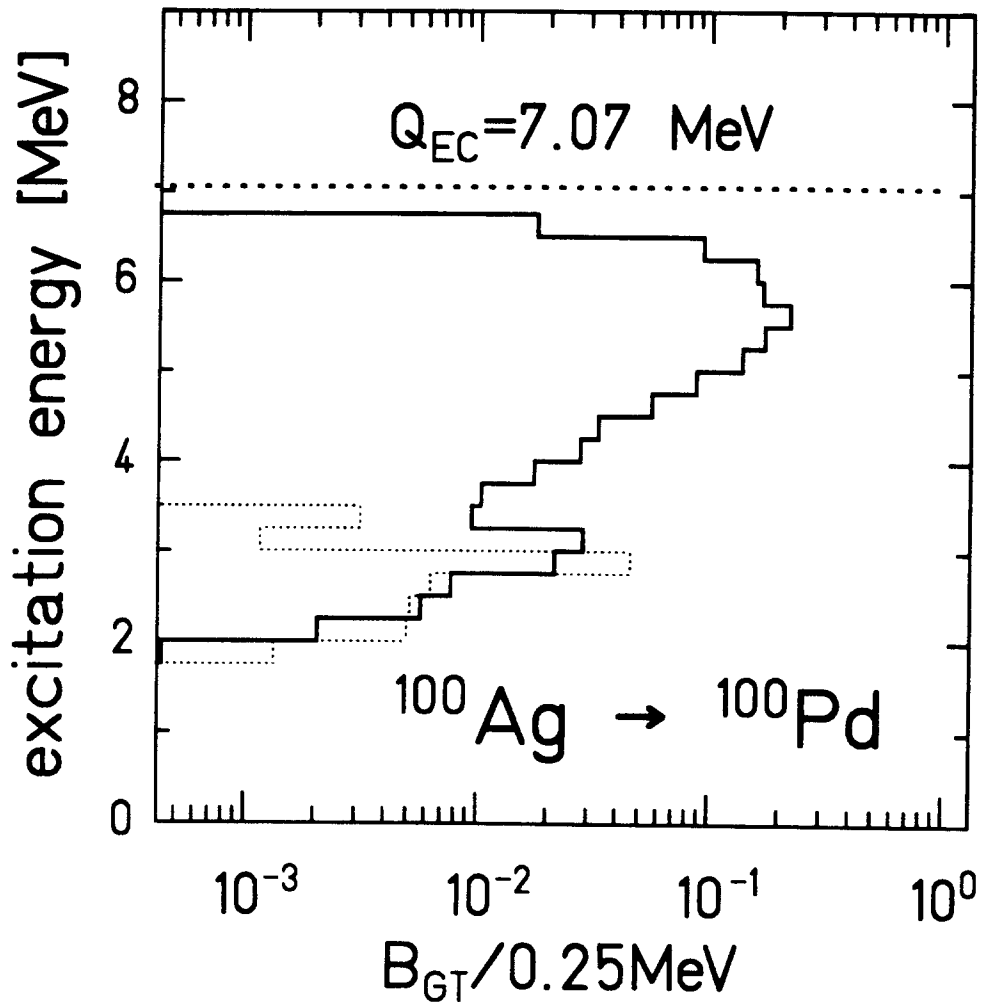

Figure 13: The GT–strength distribution determined with the TAGS [112] for the decay of ^{100}Ag (solid line). The dashed line is representing GT–strength derived from high resolution but low efficiency gamma spectroscopy experiments [113].

The best illustration how misleading might be a GT–strength picture obtained with high resolution but low efficiency gamma spectroscopy methods gives the analysis of the data on the ^{100}Ag decay [113]. In Fig.13 such results are compared to the GT–strength distribution measured with TAGS. Most of the strength (95%) have been missed in "classical" gamma counting finding only the part corresponding to the transition to relatively low–lying *2qp* state in ^{100}Pd. The upper part at the GT–strength distribution

at 5–6 MeV excitation energy found with TAGS results from the beta branching ratios of about 10% per decay (in total) and was missed in the earlier experiment [113].

It is important to notice that the total (summed) strength $B^{exp}(GT) \sim 1.9$ measured with TAGS for ^{104}In decay is larger then the value of 1.513 ± 0.055 for ^{102}Cd. The $B^{exp}(GT) \sim 1.3$ measured for ^{100}Ag matches the corresponding value of 1.21 ± 0.05 for ^{98}Pd. The nuclei $^{102}_{48}$Cd$_{54}$ and $^{98}_{46}$Pd$_{52}$ represent the even–even core for the odd–odd systems like $^{104}_{49}$In$_{55}$(^{102}Cd$\otimes\pi g_{9/2} \otimes \nu d_{5/2}$) and $^{100}_{47}$Ag$_{53}$ (^{98}Pd$\otimes\pi g_{9/2} \otimes \nu d_{5/2}$). The GT–strength distributions for ^{102}Cd and ^{98}Pd decays were studied quite precisely, including rather accurate mass measurements. Their Q_{EC} values amount to 2587 ± 8 keV and 1867 ± 25 keV, and surely quite a part of the strength is above the Q_{EC} windows and below the sensitivity limit, see section 3.3. Comparison of the TAGS data for ^{104}In and ^{100}Ag to the ones on ^{102}Cd and ^{98}Pd decays suggests that the analysis of the quenching of the total GT–strength characterizing the decays of (Z = 48, N = 54) and (Z = 46, N = 52) systems could be based also on the TAGS data on the respective odd–odd decays. Obviously, the shift of the main part of the strength towards higher excitation energies of the final states is compensated by the increase of the observation window Q_{EC}. Appropriate experimental technique, TAGS, used in the studies of odd–odd isotopes decays should enrich the systematics of GT–strength values – an input for the analysis of the origin of the quenching phenomenon.

4 Theoretical Description of the GT–Decay in the ^{100}Sn Region

The EC/β^+ decay in the ^{100}Sn region proceeds via the $\pi g_{9/2} \rightarrow \nu g_{7/2}$ GT–transformation. The elementary predictions for its GT–strength, see subsection 4.2.1, account for the single particle estimate of the square of the matrix element as well as for the number of available $g_{9/2}$ protons and $g_{7/2}$ neutron holes in the parent nucleus. However, the reference strength values obtained this way for the decays of even–even nuclei are about five times larger then the respective experimental numbers. Also, the elementary model predicts only one $0^+ \rightarrow 1^+$ $(\pi g_{9/2}^{-1}, \nu g_{7/2})$ transition in such decays, while GT–strength splitting over several final states has been established experimentally, see section 3.3. Therefore more advanced models have been applied in order to explain the measured GT–strength properties. As a first obvious step towards a better theoretical description, pairing corrections have been calculated with single–particle levels obtained in a Woods–Saxon average field and monopole pairing residual interaction, see subsection 4.2.2. However, an account for the 'advanced' approach to pairing correlations did not change much the observed quenching factors. A substantial improvement has been achieved when core polarisation (configuration mixing) effects in the ground–state of parent nucleus have been included in the model calculations (subsection 4.2.3). Also higher–order effects, e.g. Δ–nucleon hole states mixed with low–lying levels, have been considered as responsible for a part of the retardation of GT–transitions (section 4.2.4). The discreapancy between calculated and measured total GT–strength values has been quite reduced but not removed completely. Further 'strength losses' were found as due to the GT–strength distributed outside the observation windows. To account for it, the origin of the observed GT–strength splitting has been investigated - see subsection 4.2.5. A possible deformation of the states involved in the decay process has been studied, but it turned out that such states are nearly spherical. Therefore, large space spherical shell model calculations with the proton–neutron residual interaction have been performed. A satisfactory description of the relative GT–strength distribution has been finally obtained. With an account for all considered hindrance sources (see section 4.3), the distribution and magnitude of GT–strength have been quantitatively reproduced for the decays of the even N=50 isotones.

Important, new results have been also obtained for the decays of odd-tin and odd-odd indium isotopes, see section 4.4. For the experimentally studied beta–delayed proton precursors, the 'gross–properties' of their decays, like the half–life and beta-delayed proton intensity, were satisfactorily explained. Also, the major features of the GT–strength distributions for ^{100}Ag and ^{104}In, measured with the TAGS technique, have been reproduced within these shell–model calculations performed but for simpler systems with less valence nucleons, ^{98}Ag and ^{100}In, respectively.

4.1 Elementary Single Particle Shell Model as a Reference

For the orbitals involved in the $\pi g_{9/2} \rightarrow \nu g_{7/2}$ GT–transitions in the ^{100}Sn region, the angular momentum quantum number l is equal to 4. The resulting single particle estimate of such spin–flip transformation strength (cf. formula 3) is

$$B^{sp}(GT) = <\nu g_{7/2} \mid \sigma \tau^+ \mid \pi g_{9/2}>^2 = \frac{4l}{2l+1} = \frac{16}{9} \qquad (8)$$

Within the Elementary Single Particle Shell Model (ESPSM), up to ten protons can occupy the $\pi g_{9/2}$ orbit and the probability of the GT–decay of the nucleus scales proportionally to the number $N_{\pi g_{9/2}}$ of these protons, and to the square of the single proton transition matrix element $B^{sp}(GT)$. However, to get a $g_{9/2}$ proton transformed into a $g_{7/2}$ neutron one should have a free space at the $\nu g_{7/2}$ orbital. This means that the decay probability is the highest when the $\nu g_{7/2}$ state is empty (neutron number $N \leq 50$) in a given parent nucleus, and gets reduced when the $\nu g_{7/2}$ orbit is starting to be filled by neutrons.

Following ESPSM, up to eight neutrons can occupy the $\nu g_{7/2}$ state. The respective occupation coefficient can be expressed as

$$v^2_{\nu g_{7/2}} = \frac{N_{\nu g_{7/2}}}{8}, \qquad (9)$$

where $N_{\nu g_{7/2}}$ is a number of neutrons in the $g_{7/2}$ state in the parent nucleus. Finally, the ESPSM strength of the GT–decay, later on quoted as reference value, is

$$B^{ref}(GT) = \frac{16}{9} \cdot N_{\pi g_{9/2}} \cdot u^2_{\nu g_{7/2}}, \qquad (10)$$

where $u^2_{\nu g_{7/2}}$ denotes the emptiness factor for the $\nu g_{7/2}$ state,

$$u^2_{\nu g_{7/2}} = 1 - v^2_{\nu g_{7/2}} = 1 - \frac{N_{\nu g_{7/2}}}{8}. \qquad (11)$$

Within ESPSM applied to the $Z \leq 50$ and $51 \leq N \leq 64$ nuclei, $N_{\pi g_{9/2}} = Z\text{-}40$ and $N_{\nu g_{7/2}}$ depends upon the relative position of the $d_{5/2}$ and $g_{7/2}$ neutron states. If the $\nu d_{5/2}$ is lower, $N_{\nu g_{7/2}} = 0$ for $N \leq 56$, and $N_{\nu g_{7/2}} = N\text{-}56$ for larger N values up to 64. If the two states were degenerated (an approximate degeneracy is suggested by recent experimental data [36]), the neutrons above $N = 50$ would be shared by the two orbits.

4.2 Decay of Even–Even Nuclides

4.2.1 ESPSM as a Reference

For the decay of even–even nuclides in the ^{100}Sn region, the ESPSM predicts only one $0^+ \rightarrow 1^+$ $(\pi g_{9/2}^{-1}, \nu g_{7/2})$ transition. The excitation energy of this 1^+ state in the odd–odd daughter nucleus should correspond, in the naive ESPSM picture without any residual interaction, to the energy difference between the $\nu d_{5/2}$ and $\nu g_{7/2}$ orbits. This is less than 1 MeV for energies calculated with the Woods–Saxon spherical potential [114, 13]. For nuclides with $N \geq 56$ (i.e. with a full $\nu d_{5/2}$ orbital), a ground–state to ground–state decay should be observed.
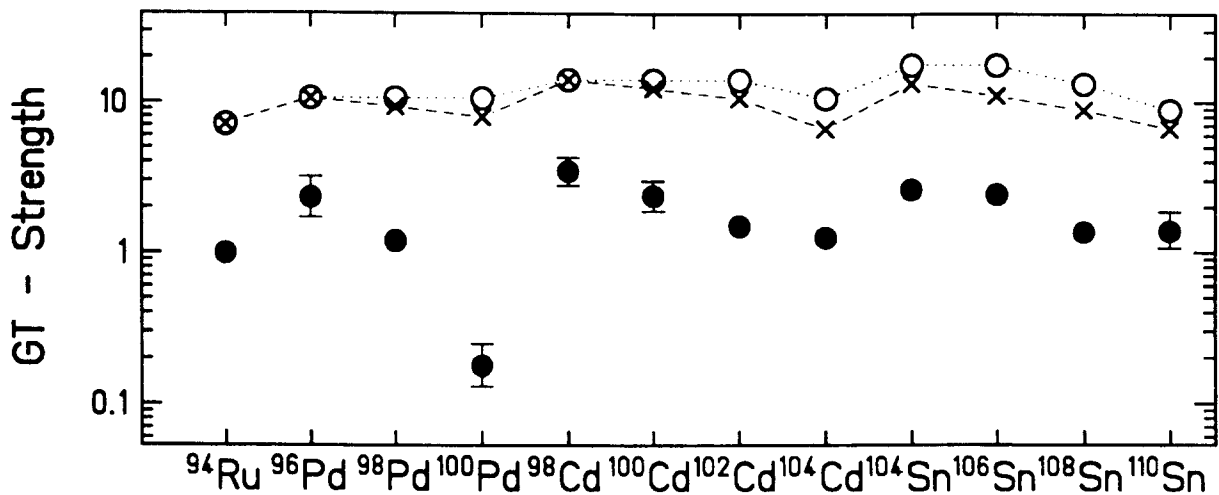

Figure 14: Experimental GT–strength (full circles) compared to the ESPSM predictions which assume either the $\nu d_{5/2}$ orbital below $\nu g_{7/2}$ (open circles) or a complete degeneracy of these orbits (crosses).

As reported in section 3.3, the decay of an even–even nuclide with high Q_{EC} reveals a few $0^+ \rightarrow 1^+$ transitions. The GT–strength, summed over the individual transitions,
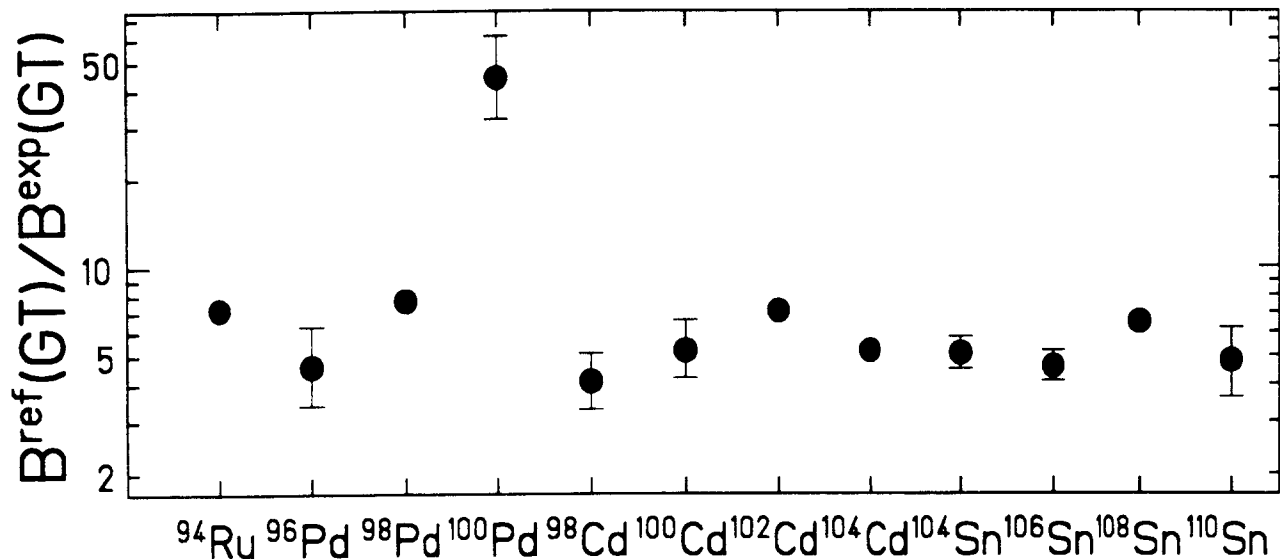
Figure 15: The ratios of the reference GT-strength $B^{ref}(GT)$ to the experimental values $B^{exp}(GT)$ are given for all studied decays of even–even nuclides in the ^{100}Sn region. For the calculation of $B^{ref}(GT)$, the energy degeneracy of the $\nu d_{5/2}$ and $\nu g_{7/2}$ orbitals is assumed (compare Fig.14).

$B^{exp}(GT)$, is much lower than $B^{ref}(GT)$. This effect of the GT–strength quenching is exhibited in Fig.14, where experimental results are compared with two sets of theoretical strength values, depending upon the relative position of the $\nu d_{5/2}$ and $\nu g_{7/2}$ states. Hindrance factors, defined as $B^{ref}(GT)/B^{exp}(GT)$ ratios, are given in Fig.15. Most of these factors are close to 5, which means that only about 20% of the GT–strength predicted by the ESPSM is found in the decays of even–even nuclides.

One point, for the ^{100}Pd decay, falls off the systematics. This is a good illustration how strong the effect of a small observation energy window can be. The value $Q_{EC} = 369 \pm 24$ keV for this decay cuts down the number of 1^+ states in ^{100}Rh available for the EC–decay to only one (at 160 keV). This state apparently carries only a small fraction of the $(\pi g_{9/2}^{-1}, \nu g_{7/2})$ configuration.

Clearly, the ESPSM is far from explaining the $B^{exp}(GT)$ data for the decays of even–even nuclides. To reproduce the observed reduction of the GT–strength, a more advanced description of nuclear structure has to be applied, see following subsections.

36

4.2.2 Pairing corrections

An obvious first step to improve the description of the GT–decay process, with respect to ESPSM, is an account for pairing correlations which allows for a better estimate of the $N_{\pi g_{9/2}}$ and $u^2_{\nu g_{7/2}}$ values used in formula 10. Now a number of $g_{9/2}$ protons to be transformed into $g_{7/2}$ neutrons is expressed as

$$N_{\pi g_{9/2}} = 10 \cdot v^2_{\pi g_{9/2}}, \tag{12}$$

where 10 is a capacity of the $\pi g_{9/2}$ orbit, and $v_{\pi g_{9/2}}$ is its occupation factor calculated for the parent nucleus.
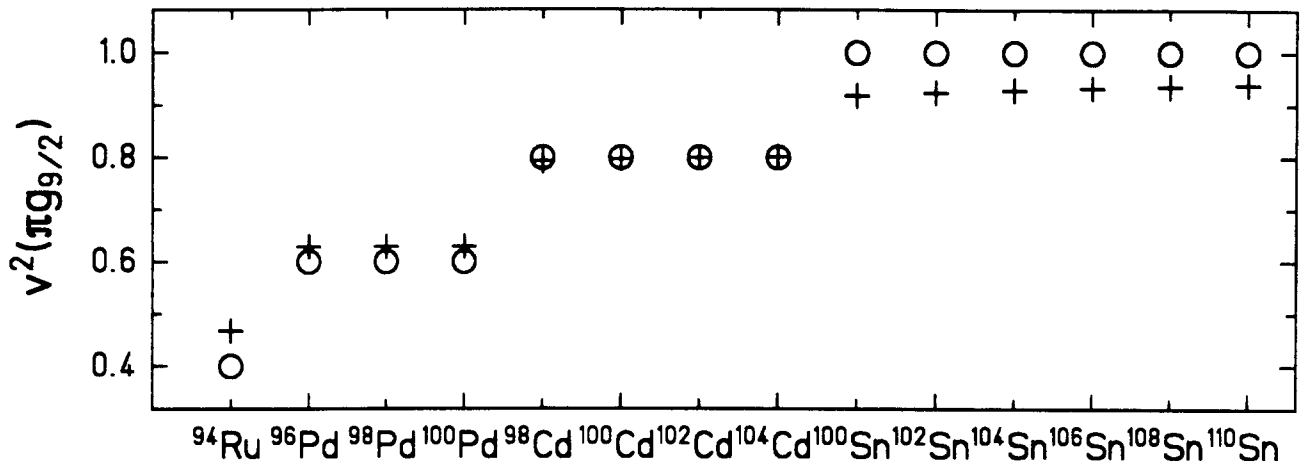

Figure 16: Occupation numbers for the $g_{9/2}$ proton orbital calculated for the discussed even–even nuclei in the ^{100}Sn region. ESPSM values (circles) are compared to those recommended in [13] (crosses), see text.

Several sets of the $v^2_{\pi g_{9/2}}$ and $u^2_{\nu g_{7/2}}$ values for even–even parent nuclei were given in [13]. The recommended ones have been obtained with the proton and neutron single-particle energies calculated in the average deformed Woods–Saxon potential [115] with the parameters taken from [116], and monopole pairing residual interaction. Total nuclear energies minimized with respect to the quadrupole (β_2) and hexadecapole (β_4) deformation parameters were calculated according to a shell correction method [117] with the Yukawa–plus–exponential mass formula [118]. The pairing energy was obtained with the Lipkin–Nogami method [119, 120, 121, 122]. As expected, the 0^+ ground-state of the discussed even even nuclei in the region of doubly–magic ^{100}Sn reveals no deformation.
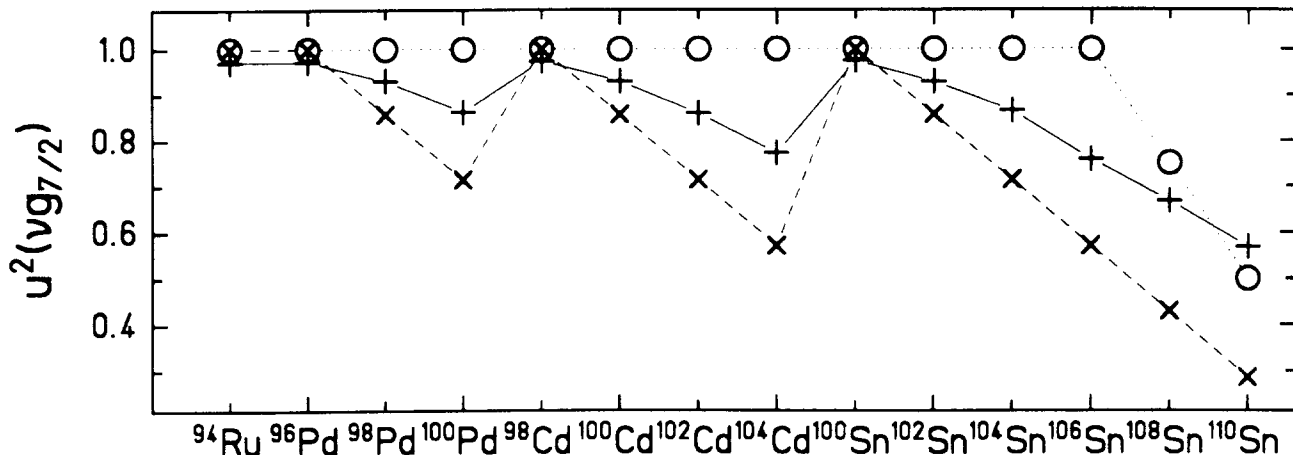
Figure 17: Emptiness factors for $g_{7/2}$ neutron orbital calculated for the discussed even-even nuclei in the ^{100}Sn region. ESPSM values calculated assuming separated $\nu d_{5/2}$ and $\nu g_{7/2}$ orbitals (circles) and degenerated ones ("X"-signes) are compared to those recommended in [13] (crosses), see text.

For the protons, see Fig.16, the computed v^2 values differ not very much from the ESPSM ones. For the neutrons, see Fig.17, the computed u^2 values lie between the ESPSM values assuming respectively separated and degenerated $\nu d_{5/2}$ and $\nu g_{7/2}$ orbitals. However, the deviation is **not significant enough** to explain the reduction by a factor of about 5 of the $B^{ref}(GT)$ values.

4.2.3 Core Polarisation

The effects related to the core polarisation of the ground–state of the parent nuclei are causing a substantial part of the quenching of the Gamow–Teller strength in the ^{100}Sn region. The main GT–strength destruction comes from the mixing within the ground–state wave function two–particle – two hole ($2p2h$) excited states resulting from breaking or exciting a pair of nucleons. The 0^+ ground–state has $2p2h$–type components, in addition to the ESPSM $0p0h$ one. These two parts of the wave function contribute with an opposite phase to the GT–matrix element, see [12, 62, 5]. Hence the transition is retarded as compared to pure ESPSM expectations.

38

In a qualitative way, one may expect that moving one or more of the $g_{9/2}$ protons through the $Z = 50$ shell gap to the other orbitals like 'GT non – active' $\pi d_{5/2}$ one reduces the number of $g_{9/2}$ protons available for the $\pi g_{9/2} \rightarrow \nu g_{7/2}$ GT – transformation. This rearrangement of the protons makes the total transition strength smaller. Within this interpretation core polarisation should have relatively more destructive influence for the decay of nuclei with a small number of $g_{9/2}$ protons than for a full $g_{9/2}$ orbit. This simple picture accounts only for a part of the *2p2h–0p0h* configuration mixing effects, but fits to the values of core polarisation hindrance factors h_{cp} obtained within advanced shell-model calculations [12, 17, 19, 20], where the magnitudes and phases of different (*2p2h*)–type excited states contributing to the ground-state configuration were taken into account.

The mixing of *2p2h* states within the 0^+ ground–state is reduced by a quite high excitation energy, at least above the energy of the magic gaps at $Z = 50$ or $N = 50$.
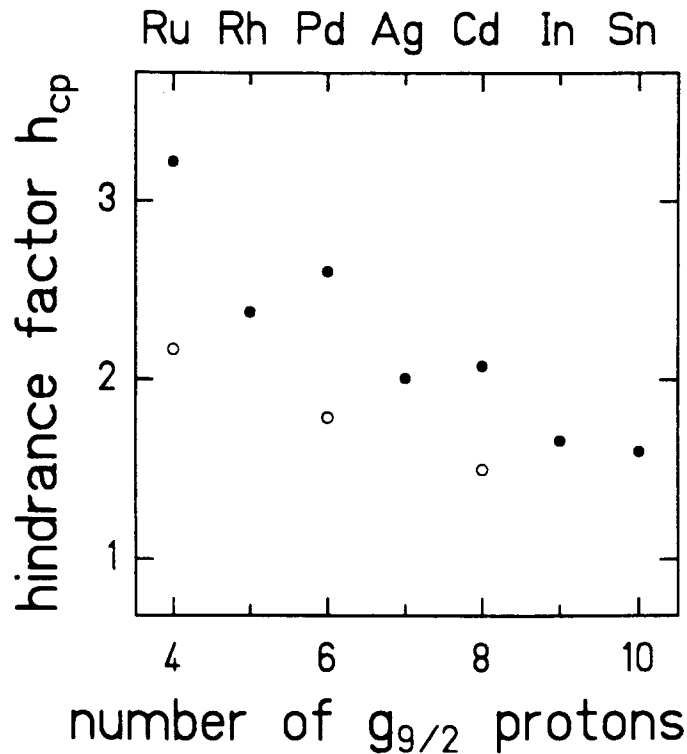

Figure 18: Core polarisation hindrance factor h_{cp} for $N = 50$ isotones calculated by Johnstone – full circles [17] and Skouras – open circles [19].

The main contribution should come from nucleon excitations to orbitals from the first subshell just above the $Z = N = 50$ cores. Among them, there is a 0^+ state having

a $4qp < 1^+(\pi g_{9/2}^{-1}, \nu g_{7/2}) \otimes 1^+(\pi g_{7/2}, \nu g_{9/2}^{-1}) >$ configuration obtained as a result of the reverse GT–transition namely $\sigma\tau^-$ operator acting on an odd–odd nucleus in the excited $1^+(\pi g_{9/2}^{-1}, \nu g_{7/2})$ state. The 0^+ ground–state of the respective even–even nuclide as well as such $4qp$ 0^+ excited state are populated in this β^- virtual transition. As discussed in [12, 62, 5], fractions of both configurations are mixed in the ground–state wave function, and contribute to GT-matrix element with opposite signes.

Some of the recently obtained h_{cp} values are given in Fig.18. The differences are mainly due to the choice of two–body interaction, of the single–particle energies and of the model space size used in the calculation. There is a clear indication (see [12, 17, 19]) that the consideration of a **Larger Model Space** i.e. a more complete picture of the nucleus, tends to **decrease the h_{cp} hindrance factors**. Values as large as $h_{cp} = 4.01$ for ^{94}Ru, 2.89 for ^{96}Pd, 2.19 for ^{98}Cd and 1.71 for ^{100}Sn decay (compare to Fig.18) were obtained by Towner [12] when 'zero–range' particle – hole interaction was used. After aplying small pairing corrections and 'higher – order' effects $h_{ho}=1.6$ hindrance (see next section), a good agreement with a limited number of measured GT – strength values was reported [12]. This was due to the compensation of the hindrance resulting from the strength splitting (see section 3.4) by the h_{cp} values. Recently calculated h_{cp} numbers are smaller (e.g. $h_{cp} = 1.25$ for ^{100}Sn [20]) leaving still some space for other quenching mechanisms, as well as for experimental reasons of missing part on the strength (sensitivity limit, Q_{EC} window), see following sections.

4.2.4 Higher–Order Effects and the Role of (Δ,Nucleon–Hole) States

An account for the hindrance factors related to pairing correlations and *2p-2h* core polarisation reduces the discrepancy between observed and calculated GT beta decay strength values for the decays of even–even nuclides. However, a full agreement is not reached, in particular when recently computed [20] h_{cp} values are applied. There are still important sources of GT-strength quenching due to the interaction (mixing) of very highly excited states with low–lying initial and final levels involved in the observed beta decay.

In addition to the transfer of a pair of nucleons across the $Z = 50$ or $N = 50$ shell gaps or nucleon–pairs break–up (i.e. core polarisation, see subsection 4.2.3) the configurations resulting from the multinucleon excitations have to be included to get "full shell–model calculations". The latter term means a complete account **only** for the first

subshell or the shell above the magic numbers $Z = N = 50$. Protons are allowed to be excited to the $\pi d_{5/2}$ and $\pi g_{7/2}$ orbitals, and neutrons may occupy $\nu d_{5/2}$, $\nu g_{7/2}$, $\nu s_{1/2}$, $\nu d_{3/2}$ and $\nu h_{11/2}$ ones. In principle, the excitations up to the full occupation of these levels and their mixing with the low–lying states have to be computed – if one aims in so called "full shell-model calculations". In reality, such approach is quite limited by practical computer time and memory restrictions affecting e.g. the maximum size of the used matrixes. The number of valence particles or/and excited orbitals is thus reduced. Qualitatively, the multinucleon excitations across the magic energy gaps are leading to the states tens of MeV above the beta decay window. Each additional excited particle increases the energy of such complex configurations. This means an increase of the energy denominator in the perturbation theory reducing the mixing of the states. However, the sum of all contributions might give a non–negligible hindrance of the GT–strength, see [24, 25, 26, 27].

Similar arguments have to be used while considering the role of the Δ–nucleon hole states [28–35]. The "classical" nuclear state is built up out of nucleons occupying a certain sequence of shell–model orbits. One may virtually replace one of the nucleons by the Δ–resonance conserving the total charge and barion number. Due to the mass difference between Δ and nucleon, such quantum system has an energy about 300 MeV above the corresponding purely nucleonic state. This means that the energy denominator scaling down the mixing between such exotic states and the classical nucleonic structures is an order of magnitude larger than for the case of the multinucleon excititations. However, the Gamow–Teller operator $\sigma\tau^+$ acting on a nucleus from the ^{100}Sn region and transferring only the protons into the neutrons, acts practically only on $g_{9/2}$ proton particles. The transformation of a proton from states below $g_{9/2}$ into the respective neutron is forbidden due to the Pauli principle (these final neutron states are fully occupied, see Fig.2). Taking as example the decay of ^{100}Sn, one finds the total ESPSM strength associated with such GT–transformation to the $1^+(\pi g_{9/2}^{-1}, \nu g_{7/2})$ state below 18, see section 3.1. In fact, this ($1h1p$) level is one of many states which could be created with the $\sigma\tau^+$ operator acting on the system of 50 protons and 50 neutrons. One gets also a spectrum of Δ–N^{-1} type states in the final ^{100}In nucleus. The up–quark (u) from each of the 100 nucleons can be transferred via the GT–operator into the down–quark (d) having the GT–selection rules fullfilled. The quantitative estimation of the total GT–probability of transitions to such Δ–N^{-1} states [45] gives

41

$B_{GT}(\Delta N^{-1}) = 24/25 * (3 * N + Z) \approx 200$ for the parent nucleus ^{100}Sn. This is an order of magnitude larger than the purely nucleonic GT–strength.

However, the level of mixing of such energetically distant states and resulting quenching of the GT–strength expected within the beta decay energy window depends upon the interaction between the Δ–N^{-1} and "classical" $1h1p$ states. This coupling strength is so far rather treated in a phenomenological way as a parameter to be fitted to the data on Gamow–Teller beta decay strength, M1 transition probabilities separated into isoscalar and isovector parts and (p,n) reaction rates [49].

For the Gamow–Teller beta–decay strength the usually adopted hindrance factor expected to account for configuration mixing with both multinucleon excitations and Δ–N^{-1} states is $h_{ho} = 1.6$ [12, 17, 20] ("ho" stays the "higher–order"). This number is based on the comparison of large scale shell–model calculations to the bulk of the experimental data for light sd–shell nuclei (mass number ranging from 17 to 40) - see [51] and earlier refs. quoted therein. The use of a hindrance factor of 1.6 is often quoted [14, 15] as renormalization of the GT–operator via the $| g_A/g_V | = 1$ renormalization of the axial to vector weak interaction coupling constants from its free neutron value of about 1.26. Application of renormalized $| g_A/g_V |$ value is equivalent to the use of a hindrance factor $(1.26)^2 \approx 1.6$. There were also attempts to estimate the effect of subnucleonic degrees of freedom in GT–transitions within the QRPA method applied to the ^{100}Sn region [35]. These results, suggesting a rather small influence of Δ–N^{-1} states on the reduction of total GT–strength, were somewhat contradictory to the conclusions based on the large scale shell–model calculations [20]. A satisfactory microscopic description of these effects, exotic for nuclear structure physics at low excitation energies, has still to be made.

4.2.5 Quenching Related to the GT–Strength Splitting

The GT–strength splitting over several final states is very well established experimentally for the decays of even–even nuclei in the ^{100}Sn region [6], see section 3.3. Also for other parent nuclei like odd–odd ^{100}Ag and ^{104}In, the spread of the beta strength over a few MeV range has been definitely concluded from experimental data taken with TAGS set–up. The recent study of the even–odd nucleus ^{105}Sn decay [107] also clearly indicates that there are quite many populated levels in the ^{105}In daughter.

Theoretical description of these experimental findings is not trivial. Even in the calculations done with models [12, 14, 15, 21] quite advanced compared to ESPSM, the resulting beta strength has been concentrated in one or two transitions.

The Role of Deformation

In addition to the study of pairing correlations, the calculations based on minimization of the total energy of the nucleus in a ground or excited state versus deformation parameters (β_2, β_4) were used to check the role of deformation as a possible cause of the observed GT-strength splitting. The decays of the even-even nuclei in the ^{100}Sn region were studied [13].

There was no deformation ($\beta_2 = \beta_4 = 0$) predicted for the $I^\pi = 0^+$ ground-states of the parent even-even nuclei – as one may expect for such systems close to the magic numbers N=50 and Z=50. A non-negligible deformation β_2 was obtained for the ground-states of the odd-odd daughter nuclei. These theoretical β_2 – values as well as the ground-state spin and parity for the neutron deficient indium isotopes were in satisfactory agreement with the experimental results derived from collinear laser spectroscopy measurements [123, 124]. A realistic description of the total energies of the ground-states of the concerned nuclei resulted also in decay energy values Q_{EC} very close to the experimentally known ones.

Static deformations of the daughter odd-odd nuclei in their excited 1^+ states were found to be very close to zero. Therefore they cannot explain the observed energy spread of the 1^+ levels (typically more than 1 MeV). The maximum splitting obtained in calculations for the 1^+ states in ^{100}Ag fed in the GT-decay of ^{100}Cd amount to 300 keV only. However, it is interesting to note that the B(GT)-weighted energies of the 1^+ states

$$< E_{1^+} >_{exp} = \frac{\sum B_i(GT) \cdot E_i^*}{\sum B_i(GT)} \quad , \tag{13}$$

were well reproduced in such calculations, particularly for the decay of cadmium isotopes, see [13]. The latter observation was later on confirmed by the experimental study of the ^{98}Cd decay [18]. This might be taken as an indication that the strength expected to be concentrated in the transition to one 1^+ level is splitted into a few ones due to the

residual interactions, but that the $B(GT)$-averaged transition energy is not changed.

In conclusion – deformation alone is **not** responsible for the observed splitting of $1^+(\pi g_{9/2}^{-1}, \nu g_{7/2})$ wave function over several levels, although one should take the deformation into account while analysing the decay energies Q_{EC} of the investigated nuclides in the ^{100}Sn region.

First Attempt to Reproduce GT–Strength Splitting

Complex shell–model calculations performed in order to explain the splitting of GT–strength, were started for relatively simple parent nuclei, namely Z=50 tin isotopes or N=50 isotones.

The first to present theoretical results explicitly showing the distribution of the GT–strength over several final states was Kalinowski [125]. The positive parity states in ^{104}In, ^{106}In and ^{108}In were generated within a model accounting for the particle–core interaction for protons and neutrons as well as for the $g_{9/2}$ proton – $g_{7/2}$ neutron interaction. This description is following to a large extent the approach of van Maldeghem and Heyde [126] applied earlier to explain the structure of the negative parity states in the heavier indium isotopes.

Even without direct inclusion of the $\pi g_{9/2}$ — $\nu g_{7/2}$ interaction term a remarkable agreement with the experimental data on low–lying $I^\pi = 2^+$ and $I^\pi = 3^+$ states has been achieved. These states were explained as built of almost pure $(\pi g_{9/2}^{-1}, \nu g_{7/2})$ and $(\pi g_{9/2}^{-1}, \nu d_{5/2})$ configurations. Most of the GT–strength was predicted to be concentrated at the lowest 1^+ state having the configuration expressed as

$$|0^+(0,0) \otimes 1^+(\pi g_{9/2}^{-1} \nu g_{7/2}); 1^+ >$$

which means a "Gamow–Teller pair" of a $g_{9/2}$ proton hole and a $g_{7/2}$ neutron particle coupled to $I^\pi = 1^+$, and coupled to the non-excited core of protons and neutrons of $I^\pi = 0^+$. The resulting spin and parity of such configuration is therefore 1^+. Already within this simple version of the presented model [125], there were additional 1^+ states at higher excitation energies resulting from the coupling of the excited proton and neutron even core (one quadrupole phonon excitation of $I^\pi = 2^+$) to the $I^\pi = 1^+$ "Gamow–Teller pair". However, in contrast to the experiment, only a small fraction of the GT–strength was predicted to appear at these higher states. This deficiency of

the model was substantially reduced with the inclusion of the $\pi g_{9/2}-\nu g_{7/2}$ interaction term. The latter interaction shifted part of the GT-strength from the lowest 1^+ level towards higher energies. For selected 1^+ levels a quantitative agreement of the excitation energies and the relative contributions to the total observed strength has been achieved by fitting only one parameter – the $\pi g_{9/2}-\nu g_{7/2}$ interaction strength [125], but for each individual decay separately.
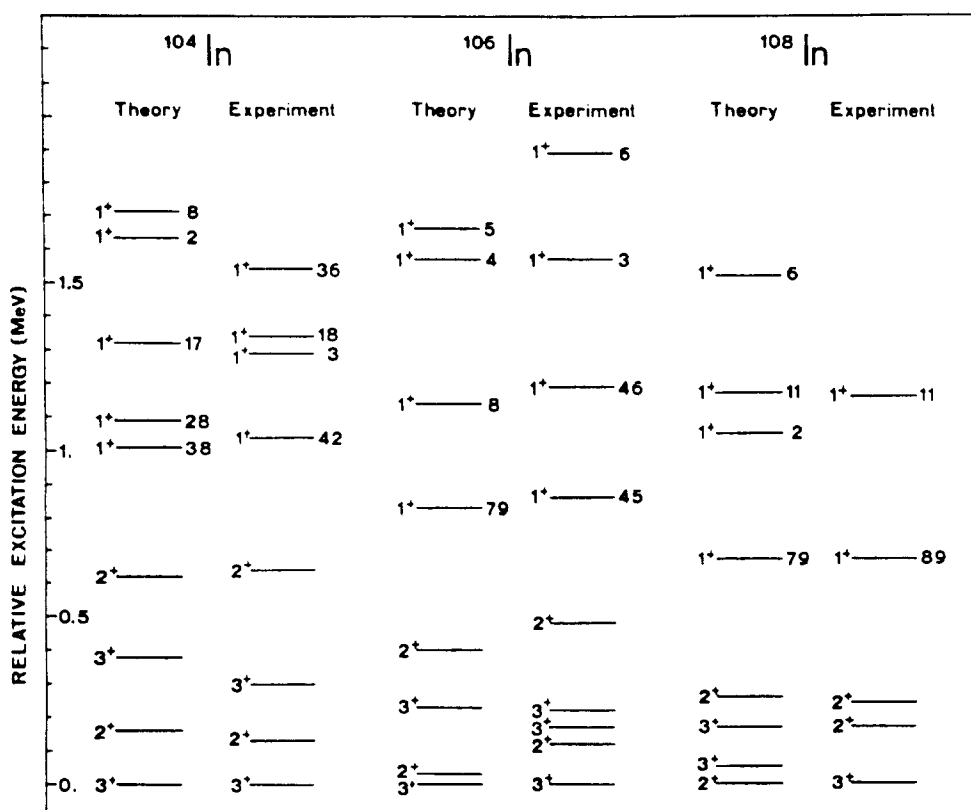
Figure 19: A comparison of energy levels calculated by Kalinowski [125] with the experimental data

The $I^\pi = 1^+$ states in ^{104}In, ^{106}In and ^{108}In were predicted at the excitation energies well below 2 MeV i.e. within the respective Q_{EC} windows, see Fig.19.

GT–Strength Splitting within the Advanced Spherical Shell–Model

The GT–decays of the very neutron deficient even tin isotopes were also studied by Brown and Rykaczewski within the large space shell model calculations [20]. This
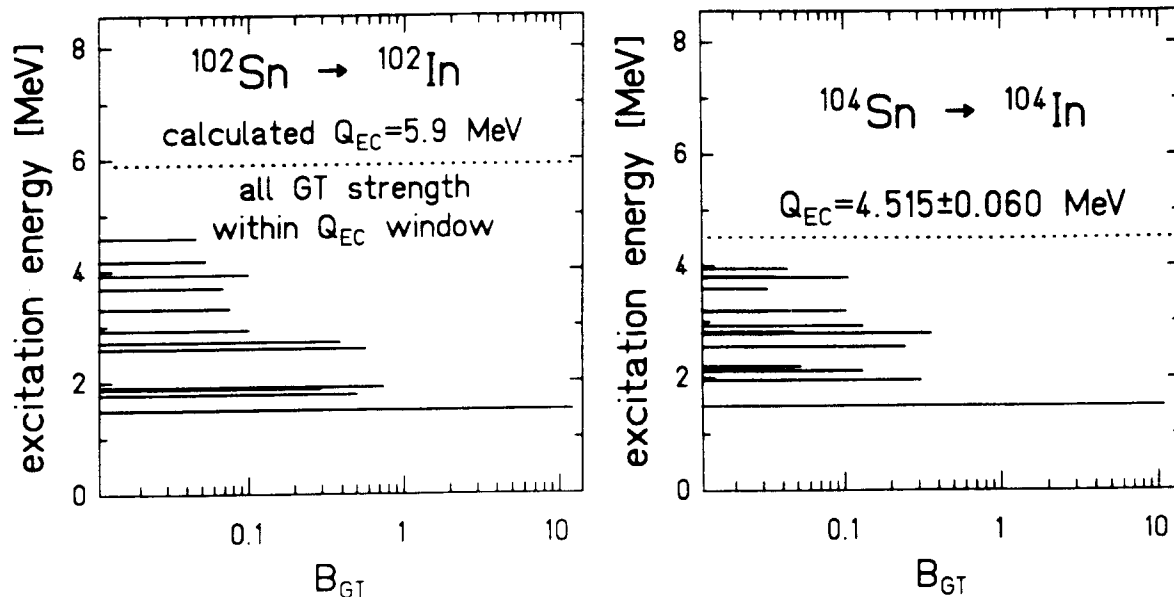
Figure 20: GT-strength distribution in the decays of ^{102}Sn and ^{104}Sn [20].

model space is designed for nuclei with $Z \leq 50$ and $N \geq 50$, and starts from a closed–shell configuration for ^{100}Sn. The active proton–hole orbitals were restricted to $1p_{1/2}$ (single-particle energy SPE $= -3.38$ MeV) and $0g_{9/2}$ (SPE $= -2.99$ MeV), since a test with the shell model space extended to the $0f_{5/2}$ and $1p_{3/2}$ orbitals did not show an essential influence on the GT–decay of ^{98}Cd. Neutron particles were assumed to occupy $0g_{7/2}$ (-10.15 MeV), $1d_{5/2}$ (-10.10 MeV), $2s_{1/2}$ (-8.40 MeV) and $0h_{11/2}$ (-7.85 MeV) orbitals. A cross–over of the $\nu g_{7/2}$ and $\nu d_{5/2}$ states is calculated to occur in ^{101}Sn (for tin isotopes having the mass number $A > 101$ the neutron orbital sequence is $\nu d_{5/2}$ below $\nu g_{7/2}$). Proton two–body matrix elements (TBME) were calculated by using the seniority–conserving interaction introduced by Gloeckner and Serduke [127], while neutron TMBE were based on results obtained by Kruse and Wildenthal [128] for $N = 82$ isotones near ^{132}Sn. The Coulomb interaction was subtracted from the $N = 82$ matrix elements and then they were scaled with a factor of $(132/100)^{0.3}$ in order to take into account the

46

change in size of the valence wave function between ^{132}Sn and ^{100}Sn. Finally, the proton–neutron interaction was calculated from the bare G–matrix according to Hosaka et al. [129], applying a scaling factor of 0.7 in order to improve the agreement between calculated and experimentally deduced $\nu g_{9/2} - \nu d_{5/2}$ SPE gap for the odd–even N = 51 nuclei.

The calculated energy spectra of 1^+ states and respective GT–strength distributions for ^{102}Sn and ^{104}Sn decays are given in Fig.20. Again the concentration of the GT–strength in the 1^+ state with the lowest exctitation energy is characteristic for the computed decays. Such feature was not found in the experimental data on the ^{104}Sn $\rightarrow$^{104}In decay, see Fig.7. The excitation energies of the 1^+ levels are above 1.5 MeV, but all states having a $(\pi g_{9/2}^{-1}, \nu g_{7/2})$ component in their wave functions are predicted to fall in the respective Q_{EC} windows.

Quite different conclusion can be drawn from several complex shell–model calculations [17, 18, 19, 20] for the decays of N = 50 isotones. The number of generated 1^+ states varied from about 10 in ^{98}Ag to over 400 in ^{94}Tc. The fraction of 1^+ levels predicted to fall into the Q_{EC} window was changing dramatically when going from ^{94}Ru towards ^{100}Sn, see Fig.21 as an example. The GT–strength within the beta decay range got close to 100% of the total expected value for ^{98}Cd decay and was smaller for lower – Z nuclei. The number of calculated 1^+ levels having a $1^+(\pi g_{9/2}^{-1}, \nu g_{7/2})$ component in their wave function is generally larger than experimentally found. However, one should note that the GT–strength characterizing some of the theoretically predicted 1^+ levels is rather small and most probably the respective beta– and following gamma–branchings were too small to be detected – see sensitivity limits in Fig.7. A quantitative comparison of the theoretical predictions to the experimental data on the N = 50 isotones decays with respect to the experimental sensitivity limits after accounting for the core polarization and the higher order effects is given in section 4.3.

However, even without taking into account for the sensitivity limits, quite some similarities can be found when comparing theoretical to experimental pictures. For the ^{94}Ru decay, the energies of two known 1^+ levels at 440 keV and 965 keV are quite accurately reproduced by the model calculations presented in [18, 19] – see also Fig.21, as well as by the results of [17]. It is also quite characteristic for all existing shell–model calculations that there is one 1^+ state in ^{94}Tc predicted at the excitation
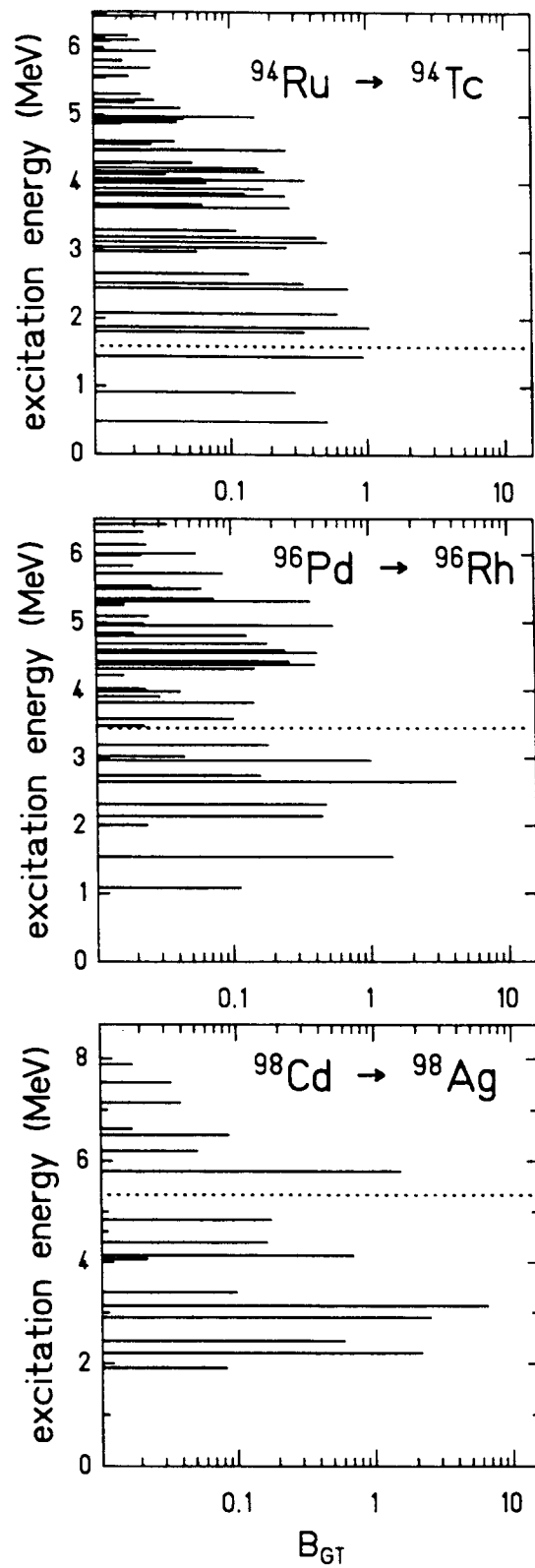
Figure 21: Energies and GT-strength of 1^+ states having a $(\pi g_{9/2}^{-1}, \nu g_{7/2})$ component calculated for $N = 51$ isotones [18,19].
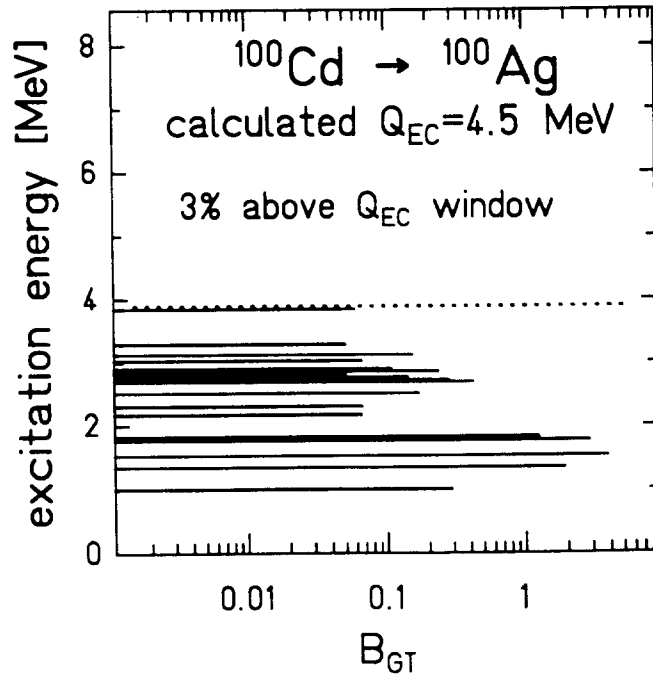
Figure 22: Calculated GT-decay of ^{100}Cd [20].

energy of about 1.5 MeV, close to the Q_{EC} limit. Due to the very low transition energy to this level, only electron-capture (EC) is possible and the absolute EC branching ratio is expected to be small. However, if one follows e.g. calculations of [19] predicting the same transition strength to this state as found already for two known 1$^+$ levels together, a detection of this state at ~1.5 MeV becomes realistic in a sensitive γ–γ experiment. Such measurements have been already proposed [130] to be performed at the Warsaw Heavy-Ion Cyclotron recently put into operation.

For the decay of ^{96}Pd. four 1$^+$ levels observed in ^{96}Rh at 939, 1275, 1565 and 1802 keV have almost one to one correspondence when comparing to the predictions of [18] and [17]. There are also states predicted by the model calculations [19] and [20] to fall in a similar excitation energy range.

Among the decays of the known $N = 50$ isotones, the ^{98}Cd$\rightarrow$ ^{98}Ag decay seems to be the best test case for the theory . Due to the largest decay energy among the known even-even nuclei near ^{100}Sn almost all of the predicted 1$^+$ levels are within reach of the beta decay. Only 2% or 7% [18. 19] of the total GT-strength is expected to be above the Q_{EC} window, while according to [20] all GT-strength is within the Q_{EC} window.

In the shell–model approach the GT–decays of the parent nuclei with the proton number Z < 50 and neutron number N > 50 are quite difficult to process. For the even–even ones only the calculations of Brown [20] for one single case (^{100}Cd decay) are existing, see Fig.21.

According to the predictions displayed in Fig.21 more then 80% of the total GT–strength is carried by five transitions to the 1^+ states at excitation energies between 1 and 2 MeV. This fits very well to the experimental data, compare Fig.7. However, the energies of 1^+ states were calculated using a Q_{EC} value of 4.5 MeV i.e. about 0.6 MeV higher than the measured one [93]. Correcting for this difference means a shift of the whole distribution by 0.6 MeV down and now seven 1^+ states fall into the 1 to 2 MeV excitation energy range, as seen in the experiment.

4.3 Advanced Theory versus Experiment for the Even–Even N = 50 Isotones

Decay properties of $^{94}_{44}$Ru$_{50}$, $^{96}_{46}$Pd$_{50}$ and $^{98}_{48}$Cd$_{50}$ are usually used as a first test of the theoretical descriptions of the Gamow–Teller beta decay in the ^{100}Sn region. The reason for that is obvious. The relatively simple systems like magic N = 50 even parent nuclei, and the daughters with only one valence neutron above the closed shell, have to be correctly described before making predictions for more complex nuclei.

In the pioneering work of Towner [12] as well as in several other approaches [14, 15, 16] only the quenching of the total GT–strength has been discussed. The basic idea of these early papers was to show that the nuclear models are able to explain the observed reduction of GT–strength. Several quenching sources have been accounted for and some parameters of the models were fitted to get the experimental strength values. The observation of several $0^+ \rightarrow 1^+$ transitions was not discussed.

In the recent shell model calculations the excitation energies of the 1^+ states and the absolute magnitudes of individual transition strength are obtained. This allows a comparison with the full experimental information – see Fig.23. These theoretical GT–spectra were obtained in two steps. Firstly, the excitation energies $E^i_{1^+}$ of the 1^+ states in the daughter ^{94}Tc, ^{96}Rh and ^{98}Ag were calculated together with their corresponding GT–strength $B_i(GT)$. The resulting GT–strength, summed over the generated spectrum of the 1^+ levels $B^{th}_{\Sigma} = \sum B_i(GT)$, was close to the ESPSM value, see

50

formula (1). The latter is due to the fact that the residual interactions (configuration mixing) in the daughter odd–odd nucleus are responsible for the distribution of the available strength over the large excitation energy range but are not reducing the total expected strength. The small deviations from ESPSM value were basically only due to different estimations of pairing effects. However, already at this stage it was clear that a part of the strength cannot be reached in the beta decay, since some of the 1^+ levels were predicted to be above the Q_{ec} window, see section 3.3.

In the second step each of the GT–strength value for the $0^+ \rightarrow 1^+$ transition was corrected by the same factor – a product of the core polarization hindrance h_{cp} calculated for the parent nucleus and the higher order hindrance h_{ho} fixed to the value of 1.6 for all considered decays. According to the present understanding this procedure should account for the main quenching mechanisms and the theoretical spectra should correspond to the observed ones. Providing it is correct, the experimental sensitivity limit can be compared to the calculated distributions. This makes it possible to deduce what fraction of the predicted $0^+ \rightarrow 1^+$ transitions, in addition to the ones above the Q_{EC} value, has been missed. The corresponding numbers are given in Fig.23.

Table 3: Summed strength of the GT–transitions observed in the decay of even $N = 50$ isotones compared to the respective values predicted within large–scale shell–model calculations. The reductions of the $B_{\Sigma}^{th}(GT)$ values due to the limited observation window (Q_{EC}, experimental sensitivity), core polarisation and higher order effects are included.

Beta Decay	$B_{\Sigma}^{exp}(GT)$	$B_{\Sigma}^{th}(GT)$			
		[17]	[18]	[19]	[20]
^{98}Cd$\rightarrow^{98}$Ag	$3.5^{+0.8}_{-0.7}$	3.3	3.6	4.9	4.9
^{96}Pd$\rightarrow^{96}$Rh	$2.33^{+0.86}_{-0.62}$	1.9	1.8	2.7	2.4
^{94}Ru$\rightarrow^{94}$Tc	$0.99^{+0.10}_{-0.08}$	0.87	0.63	0.26	0.44

The GT–strength of the transitions expected to be seen in the experiment can now be summed up and compared to the experimental value – see Table 3. The calculated numbers are not far from the experimental ones – indicating the general correctness
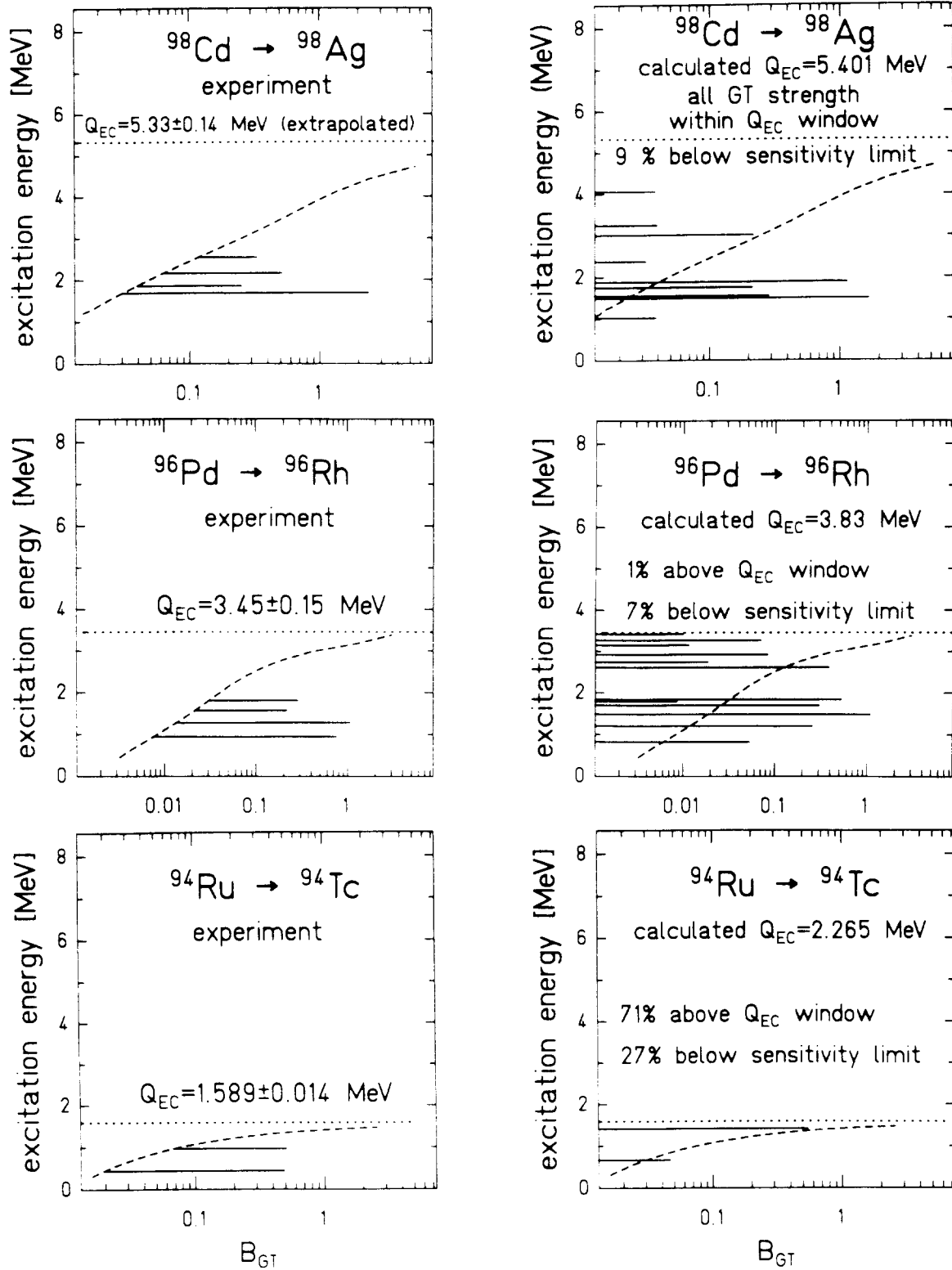
Figure 23: Comparison of the experimental and calculated [20] GT–strength distribution for the decay of $N = 50$ isotones.

of such model description of GT–decay process of these N=50 isotones. However, the microscopic calculations of h_{ho} factor for ^{100}Sn region are still to be made. There is a clear need for such hindrance factor, but e.g. the contribution of Δ–isobar excitation to h_{ho} value has to be quantitatively clarified. So far only rough estimations made for sd–shell nuclei can be quoted, and about 1/3 of h_{ho} is related to the effect of Δ – nucleon hole excitation [49]. Also the core polarization mass dependence in addition to the Z–dependence has to be investigated when coming to the neutron numbers above the closed $N = 50$ shell.

4.4 Complex Decay Patterns of 'Non Even–Even' Nuclides

4.4.1 Magnitude and Distribution of GT–Strength

The total GT–strength predicted for the decay of 'non even–even' nuclide within ESPSM is given with identical expression as for even–even ones [12]. It scales with the number of $g_{9/2}$ protons and with the single particle GT–matrix element, see formula (4). Also the method to correct ESPSM GT–strength values by hindrance factors is applicable to the decays of 'non even–even' systems. The respective core polarisation effects were calculated for odd–Z nuclei in [12] and [17] resulting in the h_{cp} hindrance factors following the general Z–dependence known for even–even systems, see example in Fig. 18. It is interesting to note that for odd–Z N=50 isotones the predicted h_{cp} values suggest somewhat smaller destructive influence on the GT–strength than for the neighbouring even–Z elements. Higher order effects, ascribed in part to the Δ – nucleon hole excitations, have also to be taken into account in order to reduce the GT–strength - as in the analysis of more simple decays.

The main difference between the decays of even–even and 'non even–even' nuclides is due to the strength distribution. Already in the ESPSM description of the decays of odd–Z nuclei having n $g_{9/2}$ protons [12], two groups of states were expected to be populated in the final nucleus. One lower in excitation energy, related to the transformation of an odd $g_{9/2}$ proton, should carry the strength:

$$B_l(GT) = \frac{2 \cdot j_> + 2 - n}{2 \cdot j_> + 1} \cdot B^{sp}(GT), \tag{14}$$

while more strength will reside at higher excitation energy, in a group of levels resulting from the GT–transformation of protons from the remaining even–proton core:

$$B_h(GT) = \frac{2 \cdot (n-1) \cdot (j_> + 1)}{2 \cdot j_> + 1} \cdot B^{sp}(GT). \tag{15}$$

With this elementary description [12] the ratio of the beta strength for the two possible decay patterns $B_h(GT) : B_l(GT)$ should be 44:1 for odd–Z indium isotopes. This prediction is not far from the values found for the decays of ^{105}In (40:1) and ^{107}In (37:1), while the experimental ratio 11:1 for ^{109}In could be interpreted as a cut of $B_h(GT)$ due to the low Q_{EC} energy, compare subsection 3.4.1. Also, such general

feature in the GT–distribution, measured with TAGS method for the [100]Ag decay, can be reproduced with the help of this simple estimations. Here, the GT–transformation of an odd–proton leads to a two–neutron configuration $\nu g_{7/2} \nu d_{/2}$ in [100]Pd, while a core decay forms fourquasiparticle states. According to formulae (13) and (14), the strength ratio $B_h(GT) : B_l(GT)$ should be 16.5:1, the experiment gives 18:1 [112]. However, such ESPSM estimation is quite far from the experimental ratio 600:1 derived for the [104]In decay from TAGS measurement. Obviously, a more advanced description of the nuclear states involved in GT–transformation, should be applied for such nuclei already distant from doubly–magic [100]Sn.
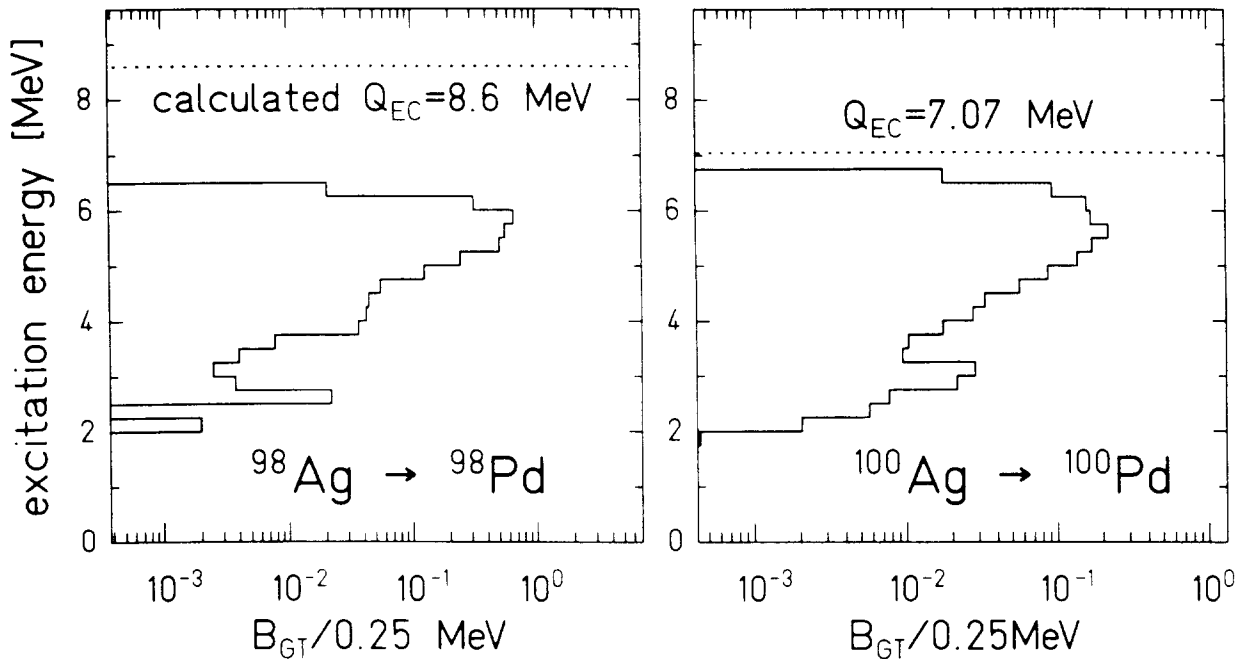
Figure 24: Comparison of the calculated GT–strength distribution for the decay of the N=51 isotone [98]Ag [20] to the strength distribution derived from the TAGS measurement for the [100]Ag decay [112].

Large scale spherical shell–model calculations, see section 4.2, have also been performed for the GT–decays of odd–A and odd–odd nuclei in the vicinity of [100]Sn [20]. In contrast to the decay of even–even nuclides, already for the closest neighbours of [100]Sn like [101]Sn and [100]In, complex and broad distributions of GT–strength were obtained. Over 100 levels in [101]In are expected to be fed in the decay of [101]Sn, and this number increases to 150 and over 300 for [103]Sn and [105]Sn decays, respectively. For the decays of

odd–odd systems like [100]In and [102]In, the numbers of levels populated in the daughter cadmium isotopes were calculated to be as high as 300 and over 1800, respectively. Unfortunately, the number of valence particles for the daughter [100]Pd and [104]Cd nuclei is too large to be processed presently in such shell–model approach, and the decays of [100]Ag and [104]In were not computed. For any of the odd–tin and odd–indium isotopes, theoretically analysed within the advanced shell–model, experimental GT–strength distributions have not been correctly (i.e. with TAGS method) obtained. However, to test the available theoretical strength distributions one may calculate such gross–properties as half–lives or beta–delayed proton branching ratios (Table 4), and compare them with relevant experimental data. Another possibility is to compare the predicted distributions with those experimentally obtained for the neighbouring heavier isotopes. The latter comparison is made in Fig.24 for [98]Ag and [100]Ag, and in Fig.25 for [100]In and [104]In. There is a resemblance between the calculated and experimental distributions.

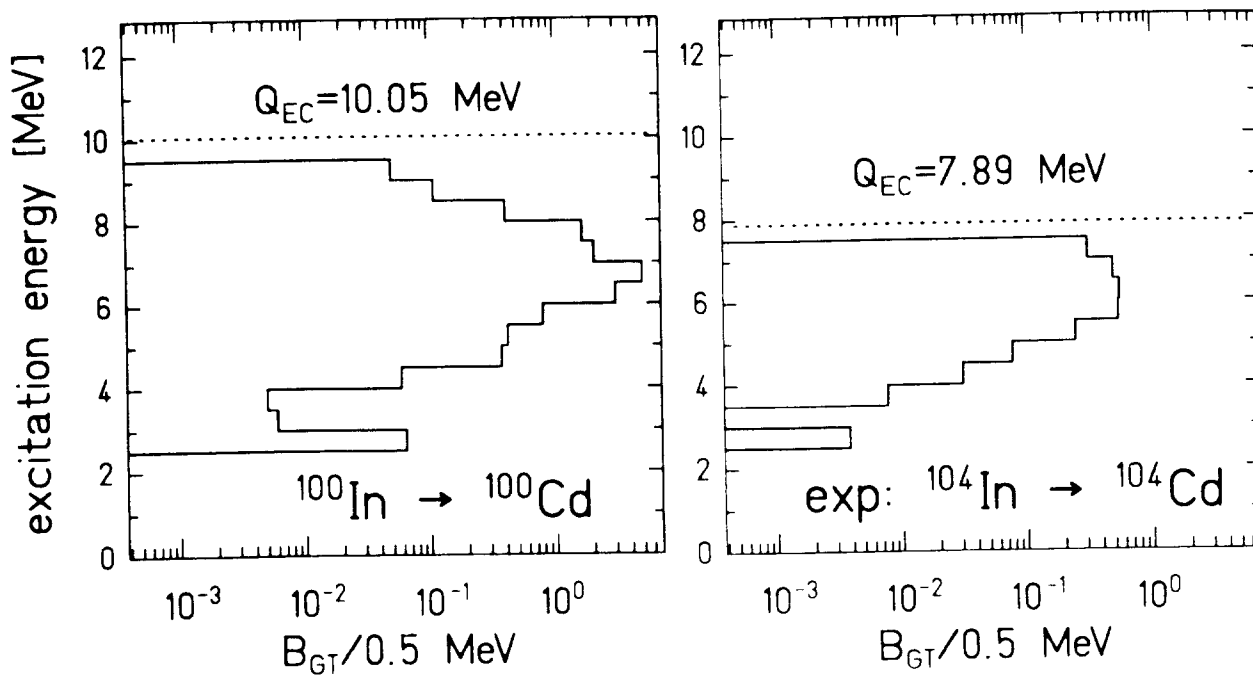
Figure 25: Comparison of the GT–strength distribution calculated for the [100]In decay [20] to the experimental (TAGS) distribution for the [104]In decay [6,107,111]

4.4.2 Decay Properties of Beta–Delayed Proton Precursors near ^{100}Sn

There are several beta–delayed proton emitters identified near doubly–magic ^{100}Sn. Such decay mode is pronounced in this region for a few reasons. With the departure from the beta stability line towards the proton–drip line, proton separation energies S_p are getting smaller. Simultaneously, the beta decay energies are increasing. In particular, the Q_{EC} values are well above 5 MeV for the very neutron–deficient odd–mass tin and odd–odd indium isotopes. Besides these favourite energy conditions, the β–delayed proton emission gets enhanced due to the dominant role of the $\pi g_{9/2} \to \nu g_{7/2}$ GT–transition and related beta decay pattern. The main part of the GT–beta decay strength is due to the transformation of a $g_{9/2}$ proton from even–even core into the $g_{7/2}$ neutron. This holds for the even–even parent nuclei **as well as** for the 'non even–even' ones. For the latter this results in final states at quite high excitation energies of a few MeV exceeding the respective S_p values. At such excitation energies the level density is high and the GT–strength is distributed over great number of levels, see Figs.11, 13.

Table 4: Decay properties of ^{101,103,105}Sn and ^{100,102}In. Experimental results [103, 106, 107] are confronted with model predictions (see text). Q_{EC} values are given for the precursors, whereas the S_p values are those of the respective daughter nuclei. $I_{\beta p}$ indicates the branching ratio for β–delayed proton emission per precursor decay.

Precursor	Q_{EC} [MeV]	S_p [MeV]	$T_{1/2}^{exp}$ [s]	$T_{1/2}^{th}$ [s]	$I_{\beta p}^{exp}$	$I_{\beta p}^{th}$
^{105}Sn	6.25(8)[a]	2.79(2)[a]	34±1	33	2.0(1)×10^{-4}	0.6(1)×10^{-4}
^{103}Sn	7.7(3)[b]	2.47(6)[a]	7.5±1.5	3.2	>0.3×10^{-2}	0.22×10^{-2}
^{101}Sn	8.9(6)[b]	1.4(3)[b]	3±1	1	−	0.2–0.4
^{102}In	8.90(33)[a]	5.48(12)[a]	22(1)	10	9.3(13)×10^{-5}	$(3.5_{-1.2}^{+5.5})$×10^{-5}
^{100}In	10.5(4)[b]	4.83(19)[a]	6.1(9)	5	>3.9×10^{-2}	(6_{-3}^{+4})×10^{-2}

a) experimental values [104]

b) values obtained by extrapolation of empirical systematics [104]

The energy spacing between these levels is well below the resolution of the particle detectors used in the decay studies (FWHM of 30–50 keV). This means an absence of the discrete proton lines characteristic for the light nuclei [131, 132, 133] and consequently bell–shaped proton energy spectrum.

Recently, the considerations presented above were described for the first time quantitatively with the help of the shell–model results [20] and of the statistical model based calculations [134, 136]. The expected GT–strength distributions for the decays of ^{101}Sn, ^{103}Sn and ^{105}Sn as well as for ^{100}In and ^{102}In isotopes are presented, respectively, in Fig.26 and Fig.27 together with Q_{EC} and S_p energies. The same two–step correction procedure, as for the analysis of the decays of even $N = 50$ isotones (see section 3.7.1), has been applied to get strength values which could be compared to the experiment. Experimentally determined "gross–properties" of beta decay like the halflives and beta–delayed proton branching ratios have been confronted with the theoretical predictions in Table 4.

For such a comparison it is important to notice that the GT–strength distributions presented in Fig.26 and Fig.27 have been obtained **relative to the ground state of the parent nuclides.** The beta transition energy and associated strength has been calculated for each contributing transition. This means that the resulting halflives are not affected by the Q_{EC} values, separately computed within the same shell–model approach. These halflives are, of course, affected by the hindrance factors used to correct "raw" strength values.

The expectation was that calculated Q_{EC} and $T_{1/2}$ values reproduce better the measured data for "simpler" nuclei i.e. those closer to the magic numbers. While the prediction for ^{100}In is in quite good agreement with experiment, the two–neutron heavier one, ^{102}In, is predicted to have a half–life shorter than found experimentally, see Table 4. This may indicate an A–dependence of the core polarisation hindrance factor (in addition to the theoretically known Z–dependence). A similar $T_{1/2}(th)/T_{1/2}(exp)$ dependence was found for ^{98}Cd and the two–neutron heavier ^{100}Cd; the theoretical to experimental half–life ratio was 0.91:1 and 0.62:1, respectively. However, the computed halflives of the chain of tin isotopes surprisingly do not confirm such behaviour. Obviously, the $h_{cp}(Z, A)$ function needs more theoretical studies. In particular, the GT–strength distributions should be calculated for decays of other nuclides, having $N > 50$.
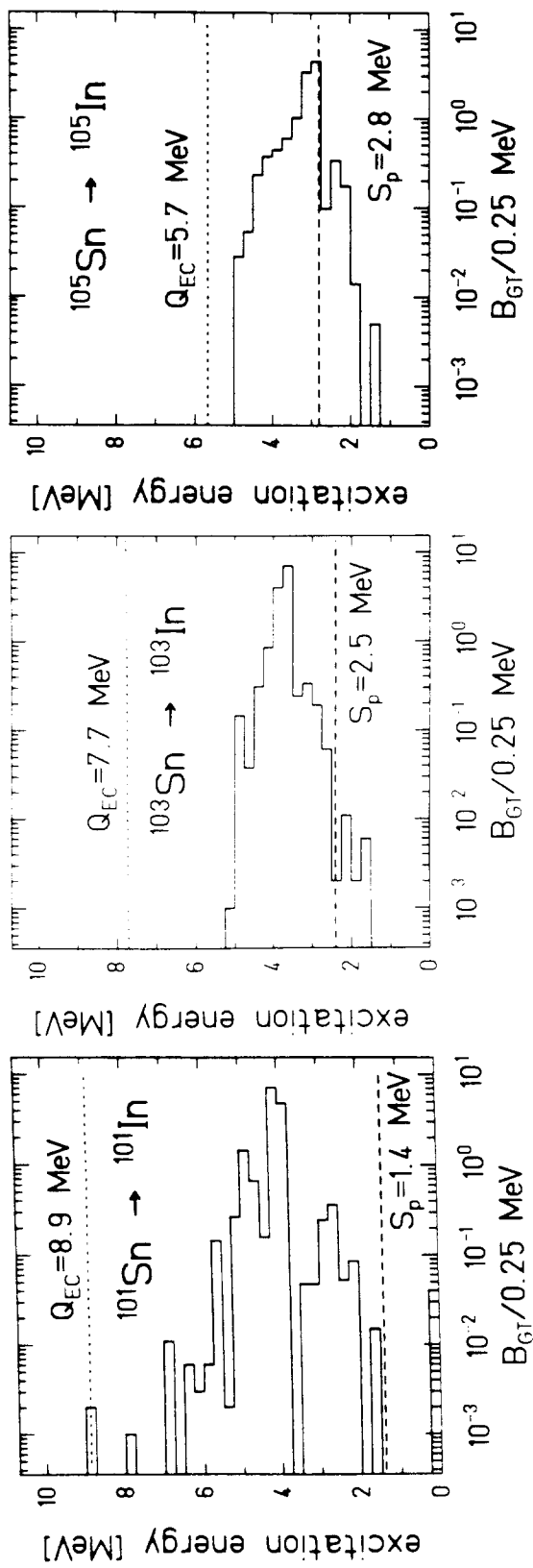
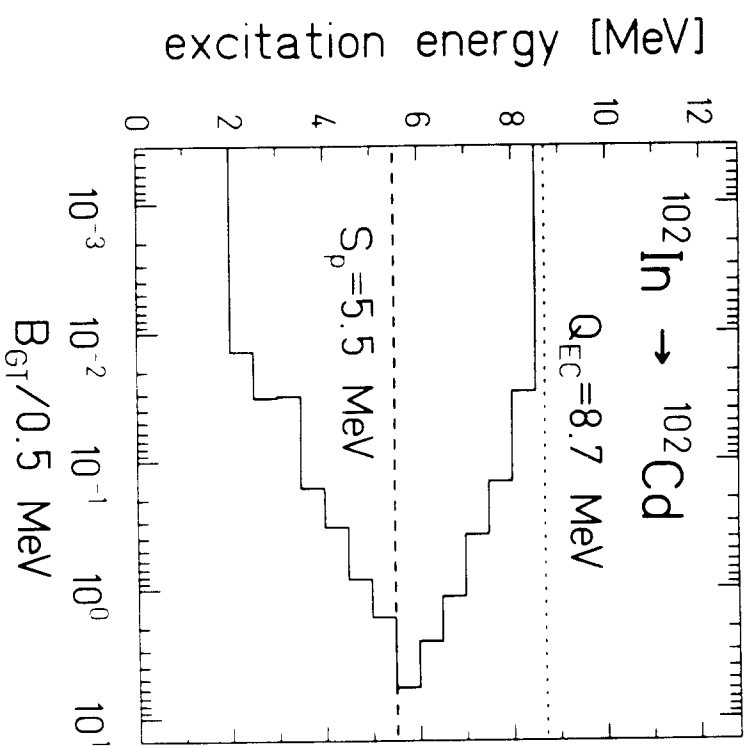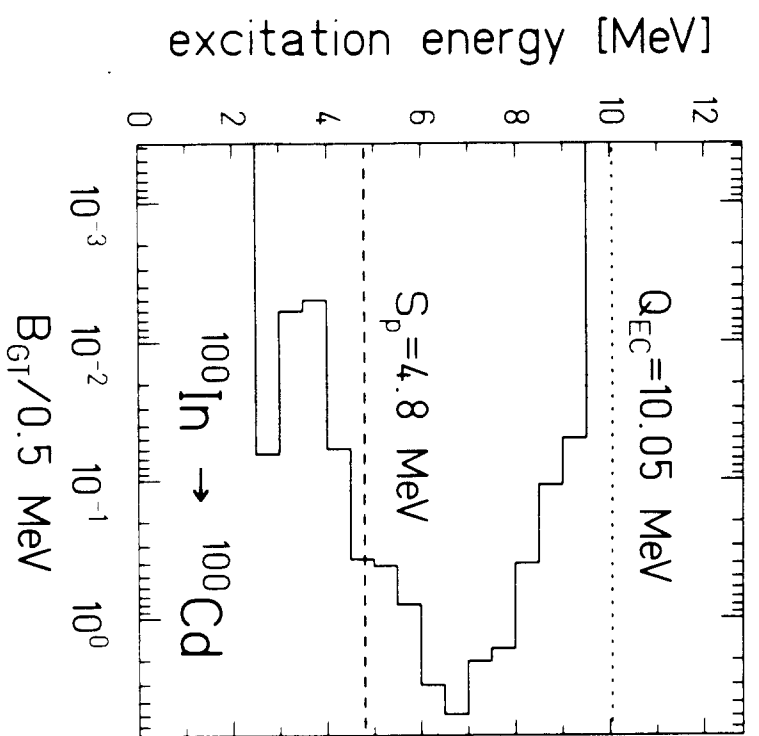Figure 26: Calculated GT-strength distributions for the decay of neutron deficient odd-mass tin isotopes [20].

Figure 27: Calculated GT strength distributions for the decay of neutron deficient odd odd indium isotopes [20].

In some cases like ^{100}In and ^{105}Sn, it seems that the beta transition energies and strength distributions are predicted correctly (see $T_{1/2}^{exp}$ vs $T_{1/2}^{th}$, Table 4), but that the calculated Q_{EC} values differ from the experimental or semi–experimental systematic values, compare Q_{EC} energies given in Fig.26 and Fig.27 with respective ones in Table 4. Presumably, this might be due to a similar deformation (or absence of deformation) of the parent and daughter GT–states while the ground–state of the daughter nucleus is more deformed. So far the calculations confirming this statement were only performed for even–even nuclei decays [13], where 0^+ parent states and 1^+ final states had practically no deformation. However, also for 'non even–even' ones the decay is associated with the transformation within the even–even core, which suggests at least similar (not necessary zero) deformations of parent and daughter GT–states also for 'non even–even' decays in the ^{100}Sn region. This may lead to a correct calculation of the beta transition energies and a wrong calculation of the decay energies.

Calculations of beta–delayed proton branching ratio require several input parameters like energies of involved nuclear states, penetrabilities of the Coulomb barrier (strongly dependent on barrier parametrization) and beta–feeding intensity distribution. Competition with other deexcitation ways (mostly gamma decay) has to be accounted for. Therefore it is difficult to draw a conclusion in case of disagreement with an experimental value. However, the good agreement for several computed decays, compare Table 4, may indicate the general correctness of the model and input parameters used, including the calculated beta strength function. One should note that the beta–delayed proton branching ratio is changing by about two orders of magnitude when removing two neutrons out of the precursor nucleus. Therefore a reproduction of the observed absolute values within a factor of a few could be quoted as a success of the model. The predictive power of the calculations seems to be already meaningful for planning further experiments.

5 Summary and Conclusions

The decay studies in the region of the doubly–magic nucleus ^{100}Sn, described in this paper, were performed for more than twenty nuclei . The experiments were carrried out at the on–line mass–separators at GSI Darmstadt, CERN Geneva (ISOLDE) and Louvain–la–Neuve laboratory (LISOL). The experimental techniques included high-resolution γ–ray and X–ray spectroscopy as well as 4π–total absorption gamma measurements. The energy spectra of charged particles like conversion electrons, positrons emitted in the β^+–decay and β–delayed protons were also recorded.

New or substantially improved partial decay schemes were obtained for ^{103,104,105,106,108}Sn, ^{101,102,103,104}In, ^{98,100,102,104}Cd, ^{100}Ag and ^{96,98,100}Pd. For the first time in the ^{100}Sn region, GT strength distributions were derived for the decay of odd–odd nuclei like ^{100}Ag and ^{104}In. The main decay properties, the half–life and the beta-delayed proton branching ratio, were measured for the very neutron–deficient isotopes ^{101,103,105}Sn, ^{100,102}In, ^{97}Cd and ^{94,95}Ag [53, 135]. For all these nuclides, the beta decay has been interpreted as dominated by the $\pi g_{9/2} \rightarrow \nu g_{7/2}$ Gamow–Teller transformation. The splitting and quenching of the GT transition strength have been established.

A number of theoretical studies has been stimulated by these experimental data. Particular attention has been devoted to the origin of the retardation of the observed $\pi g_{9/2} \rightarrow \nu g_{7/2}$ GT transitions. The role of pairing correlations, deformation and explicitely of the $g_{9/2}$ proton–$g_{7/2}$ neutron residual interaction was studied. Good agreement with the experimental strength distribution has been achieved by using advanced, large scale shell–model calculations, in particular for the decays of even N=50 isotones. Since such calculations are limited to systems with only few valence particles, the GT–strength distributions determined experimentally for the ^{100}Ag and ^{104}In decays could only be compared with shell–model predictions for ^{98}Ag and ^{100,102}In. The measured halflives and beta–delayed proton branching ratios were satisfactorily reproduced for a number of very neutron–deficient nuclei. However, the phenomenological value of the 'higher–order' hindrance factor h_{ho} of 1.6 had to be applied in such calculations. The 'higher–order' hindrance might at least partly be due to the mixing of low–lying levels with Δ–particle nucleon–hole states. Correspondingly, the subnucleonic degrees of freedom have to be taken into account in the interpretation of the GT-strength properties near ^{100}Sn.

The predictive power of the large scale shell–model calculations can be tested by using the ^{100}Sn β–decay half–life that became available recently: the computed values are 0.53 s [20], see Fig. 28, and 0.6 s [22], while the first experimental estimate [100] yields $T_{1/2}(^{100}\text{Sn}) = 0.66^{+0.59}_{-0.22}$ s.

In conclusion, the GT–beta decay and structure of nuclei in the ^{100}Sn region have been understood well enough to make reliable estimates of the gross beta decay properties. However, an unambiguous interpretation of the 'higher–order' hindrance is still needed, including a microscopic estimate of a possible contribution related to the subnucleonic degrees of freedom.
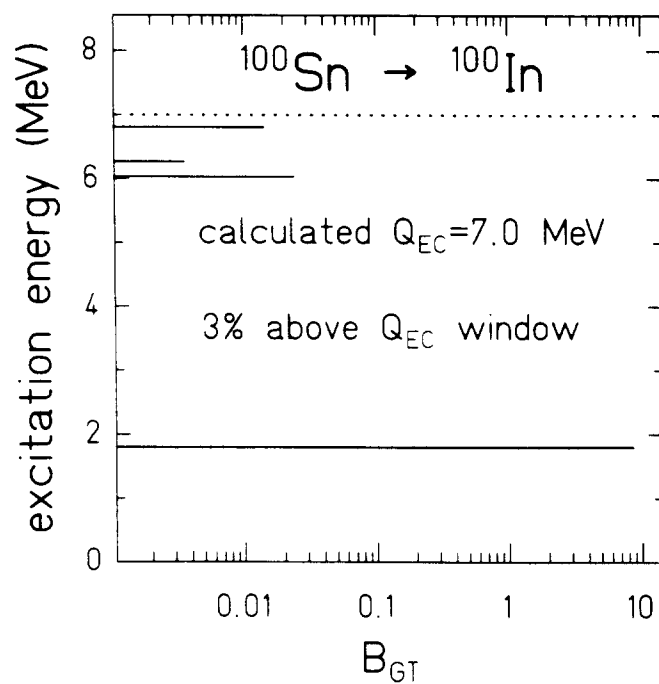

Figure 28: Calculated GT–strength distribution for the decay of ^{100}Sn [20]

6 Perspectives of Further Studies

The program of the systematic experimental studies of beta–decay near ^{100}Sn can be somewhat arbitrarily divided into three subsequent steps. The first one aims at the production and identification of the exotic nuclei of interest. The second group of measurements is focussed onto the basic decay properties. During the most difficult but also most conclusive third step the 'precision investigations' are carried out.

Presently, the studies of nuclei near ^{100}Sn are in the phases two and three of this program. All nuclei situated 'south–east' from ^{100}Sn, and ^{100}Sn itself, have been identified among the the fusion–evaporation and quasifragmentation reaction products. Some additional information on nuclear structure near doubly–magic ^{100}Sn has been gained from the studies of charged particle and heavy–ion radioactivity like the ground–state emission of protons, and alpha [86, 87, 137] and ^{12}C particles [138, 137]. A few decays, namely ^{98}Pd, ^{102}Cd and ^{100}Ag, have been studied on 'precision level'. These results together with gross decay information on other nuclei, including more exotic ones like ^{98}Cd, allowed to make reliable predictions for yet unknown decays, and to interpret the observed properties within a 'partially microscopic–partially phenomenological' approach.

With the installation of an LED–stabilized total absorption gamma spectrometer at the GSI on-line mass separator [139], new possibilities for the investigations of 'non even–even' nuclei have opened up. This set-up, combined with chemically selective ion-sources operational at GSI ISOL, will be used already in Summer 1995 for the decay studies of very neutron–deficient indium and silver isotopes including ^{102}In and ^{98}Ag [8].

In the near future the studies performed at the on–line mass separator should also improve the data on the main input parameters necessary to derive $B(GT)$ values for even–even nuclides. The $T_Z = 3$ nuclides ^{98}Pd, ^{102}Cd and ^{106}Sn have been already investigated rather precisely (with the exception of Q_{EC} energy for ^{106}Sn known with an accuracy of 60 keV, the latter decay planned to be restudied at the Warsaw Cyclotron facility).

For the $T_Z = 2$ nuclei ^{96}Pd, ^{100}Cd and ^{104}Sn, the decay energy should be remeasured and the gamma detection limit should be improved to reach the precision level. For

all three cases, this is already now possible at the on–line mass separators at GSI or ISOLDE/CERN. An application of the presently available chemically selective ion–source techniques [73, 72] combined with the advanced spectroscopy equipment like the summation–free beta–endpoint spectrometer or the LED–stabilized total absorption gamma spectrometer should help to achieve an improved accuracy.

A rich information on the levels populated in the decay of the $T_Z = 1$ nuclide ^{98}Cd was already obtained. However, an extrapolated Q_{EC} energy was used to derive $B(GT)$ value, and it should be replaced by an experimental one. First measurements of the production rates of very neutron–deficient cadmium isotopes at the new ISOLDE/PS Booster facility are planned for October 1995. To measure the decay properties of the next $T_Z = 1$ nucleus, ^{102}Sn, it is necessary to improve the efficiency of the existing laser ion–source. Such an improvement seems to be possible [140], but requires further tests and technical developments.

Even with all these improvements in the mass separator technique, it will be ex–tremaly difficult to obtain data on the decay of the $T_Z = 0$ nuclide ^{100}Sn. However, new perspectives have been opened for nuclear spectroscopy in the ^{100}Sn region due to the radioactive beam techniques. In 1994, the experiments using the relativistic heavy–ion beams for the studies of nuclei near ^{100}Sn have been succesfully completed at FRS (GSI) [1, 100] and LISE (GANIL) [2, 3]. Among the highligths of the FRS experiment, performed by using fragmentation reactions induced by a ^{124}Xe beam at 1.1 GeV/nucleon, are (i) the identification of ^{100}Sn, (ii) the first experimental informa–tion on the half–life of ^{100}Sn, and (iii) even some very rough information on the energies of emitted positrons.

By using quasifragmentation reactions of a ^{112}Sn beam at intermediate energies, seventeen new isotopes, i.e. ^{103,104,105}Sb, ^{102}Sn, ^{98,99}In, ^{94,95}Ag, ^{91,92,93}Pd, ^{89,90,91,92,93}Rh and ^{87,88}Ru were identified among the reaction products. As the main result of this experiment, twenty four events were assigned to the doubly–magic nucleus ^{100}Sn. The predicted proton drip–line has been reached for the indium and silver isotopes and even crossed for the antimony and rhodium isotopes.

Continuation of these studies is foreseen, both at GSI and GANIL projectile frag–ment separators, with a focus on the decay properties of ^{100}Sn. The measurements with

a large, position–sensitive silicon detector surrounded by a sensitive gamma detection set-up are planned at GANIL. The distribution of the quasifragmentation products over a large, segmented detector should allow for a correlation (in the prompt and slow mode) between the implanted ions with and the following beta and gamma radiation i.e. to investigate the decay scheme of ^{100}Sn. The high–intensity injector to the UNILAC–SIS accelerator complex will increase the available primary beam intensities and corresponding rates of exotic fragmentation products at the FRS facility. The atomic mass of ^{100}Sn will most probably be measured in the near future using the two–cyclotron method [78, 141] at GANIL. By combining the results obtained by using fragmentation of relativistic projectiles and fusion–evaporation reactions, it may be possible to obtain the GT-strength for the decay of the doubly–magic ^{100}Sn, and hopefully to improve our knowledge on the renormalization of the axial vector coupling constant g_A.

7 Acknowledgements

At present the success of a large experimental program in nuclear physics is related to the collaboration of a group of people, including physicists, engineers, technicians, accelerator and computer experts. They all contribute to the project. Here I would like to thank my colleagues for participating through the many days and nigths devoted to the experiments on the study of the ^{100}Sn region:

– to members of the Nuclear Spectroscopy Group at Warsaw University led by prof. Jan Żylicz, including prof. Andrzej Płochocki, Drs. Jurek Szerypo, Zenon Janas and Marek Pfützner and most recently MSc. Robert Grzywacz. Particularly I would like to express my thanks to prof. Jan Żylicz, who triggered this scientific program and directed my attention to the problem of the GT-transitions, for many hours of the enlightning discussions and a great help at all phases of the project,

– to the members of the GSI on–line mass separator group led by prof. Ernst Roeckl, including Dr. Reinhard Kirchner and his team of experienced 'msep drivers' – Karl–Heinz 'Charlie' Burkard, Wilfried Hüller, Christoph Bruske, Karl–Heinz Behr and Adolf Brunle. Drs. Otto Klepper, Dieter Schardt, Sissy Rathke, Raimund Barden and Horst Keller, and MSc. Karsten Schmidt for sharing much excitement while watching new activities appear on the computer screen,

– to the members of the LISOL group of KU Leuven led by prof. Mark Huyse, including prof. Piet Van Duppen and Drs. Geert Reusen and Jan Wauters, the partners you may always depend on,

– to the members of the ISOLDE Collaboration at CERN, particularly to profs. Hans–Jürgen Kluge, Heinz Haas, and Piet Van Duppen, for supporting our studies

References

[1] R. Schneider, J. Friese, J. Reinhold, K. Zeitelhack, T. Faestermann, R. Gernhauser, H. Gilg, F. Heine, J. Homolka, P. Kienle, H. J. Körner, H. Geissel, G. Münzenberg and K. Sümmerer; Z. Phys. **A348** (1994) 241

[2] M. Lewitowicz, R. Anne, G. Auger, D. Bazin, J. M. Corre, R. Hue, M. G. Saint–Laurent, R. Grzywacz, M. Pfützner, K. Rykaczewski, J. Żylicz, A. Fomichov, S. Lukyanov, Yu. Penionzkevich, O. Tarasov, V. Borrel, D. Guillemaud–Mueller, A. C. Müller, F. Pougheon, O. Sorlin, C. Borcea, Z. Janas, H. Keller, T. Dörfler, W. D. Schmidt–Ott, M. Huyse, J. Szerypo, and J. Wauters; Phys. Lett. **B332** (1994) 20

[3] K. Rykaczewski, R. Anne, G. Auger, D. Bazin, C. Borcea, V. Borrel, J. M. Corre, T. Dörfler, A. Fomichov, R. Grzywacz, D. Guillemaud–Mueller, R. Hue, M. Huyse, Z. Janas, H. Keller, M. Lewitowicz, S. Lukyanov, A. C. Müller, Yu. Penionzkevich, M. Pfützner, F. Pougheon, M. G. Saint–Laurent, K. Schmidt, W. D. Schmidt–Ott, O. Sorlin, J. Szerypo, O. Tarasov, J. Wauters and J. Żylicz; "Identification of New Nuclei at and beyond the Proton Drip–Line near the Doubly–Magic Nucleus ^{100}Sn", GANIL Preprint P 94 30, submitted to Phys. Rev. Lett.

[4] P. E. Haustein (ed.); At. Data Nucl. Data Tables **39** (1988) 185

[5] J. Żylicz; Proc. of the XXth Winter School "Selected Topics in Nuclear Structure", Zakopane, Poland, 13–26 April 1985, Report IFJ No 1302/PS, Kraków 1985, p. 164

[6] K. Rykaczewski; in Proc. of 6th Int. Conf. on Nuclei Far From Stability and 9th Int. Conf. on Atomic Masses and Fundamental Constants, Bernkastel–Kues 1992, R. Neugart, A. Wöhr (eds), IOP Conf. Ser. **132** (1993) 517

[7] K. Rykaczewski (speaker); GSI Proposal **U072**, Berlin – CERN – GSI – Leuven – Mainz – Troitzk – Warsaw Collaboration, "Towards Doubly–Magic ^{100}Sn: The Identification and Studies of Gamow–Teller Beta Decay of ^{102}Sn", 1991, and earlier proposals 1980–1990

[8] K. Rykaczewski (speaker); GSI Proposal **U085**, Berkeley – Berlin – Darmstadt – Leuven – St. Petersburg – Warsaw Collaboration, "Towards Doubly–Magic ^{100}Sn:

Investigation of the beta decay of neutron–deficient indium isotopes by means of total absorption gamma–ray spectroscopy", 1992

[9] K. Rykaczewski (speaker); ISOLDE/CERN proposal **IP01-50**, Berlin – Darmstadt – Geneva – Warsaw Collaboration, "Determination of Decay Energy and Gamow–Teller Strength for the ^{98}Cd Decay", 1990

[10] K. Rykaczewski (speaker); ISOLDE/CERN proposal **ISC/P55**, Aarhus – Berlin – Darmstadt – Geneva – Jyvaskyla – Warsaw Collaboration, "Towards the Proton Drip–Line along the Cadmium Isotopic Chain", 1993

[11] K. Rykaczewski (speaker); GANIL – Warsaw – Dubna – Orsay – GSI – Bucharest – Leuven Collaboration, proposal to GANIL Comite d'Experiences, June 1993, GANIL Report 93 06, p.70

[12] I. S. Towner; Nucl. Phys. **A444** (1985) 402

[13] J. Dobaczewski, W. Nazarewicz, A. Płochocki, K. Rykaczewski and J. Żylicz; Z. Phys. **A329** (1988) 267

[14] J. Suhonen, T. Taigel and A. Faessler; Nucl. Phys. **A486** (1988) 91

[15] V. A. Kuzmin and V. G. Soloviev; Mod. Phys. Lett. **A3** (1988) 1533

[16] I. N. Borzow, E. L. Trykow and S. A. Fayans; in Proc. of 6th Int. Conf. on Nuclei Far From Stability and 9th Int. Conf. on Atomic Masses and Fundamental Constants, Bernkastel–Kues 1992, R. Neugart, A. Wöhr (eds), IOP Conf. Ser. **132** (1993) 651

[17] I. P. Johnstone; Phys. Rev. **C44** (1991) 1476

[18] A. Płochocki, K. Rykaczewski, T. Batsch, J. Szerypo, J. Żylicz, R. Barden, O. Klepper, E. Roeckl, D. Schardt, H. Gabelmann, P. Hill, H. Ravn, T. Thorsteinsen, I. S. Grant, H. Grawe, P. Manakos, L. D. Skouras and the ISOLDE – Collaboration; Z. Phys. **A342** (1992) 43

[19] L. D. Skouras and P. Manakos; J. Phys. **G19** (1993) 731

[20] B. A. Brown and K. Rykaczewski; Phys. Rev. **C50** (1994) R2270

[21] I. N. Borzow, S. A. Fayans and K. Rykaczewski; Bull. Russ. Acad. Sci. Phys. (USA) **57** (1993) 1783

[22] I. Hamamoto and H. Sagawa; Phys. Rev. **C48** (1993) R960

[23] J. Schaffner, J. A. Maruhn, H. Stoecker, W. Greiner; Z. Phys. **A350** (1994) 91

[24] J. M. Irvine, G. S. Mani, V. F. E. Pucknell, M. Vallieres and F. Yazici; Ann. Phys. (NY) **102** (1976) 129

[25] I. S. Towner; Prog. Part. Nucl. Phys. **11** (1984) 91

[26] A. Abbas, F. Beck and A. Richter; Z. Phys. **A321** (1985) 329

[27] A. Abbas; J. Phys. G:Nucl. Phys. **15** (1989) 793

[28] M. Ericson, A. Figureau and C. Thevenet; Phys. Lett. **B45** (1973) 19

[29] M. Rho; Nucl. Phys. **A231** (1974) 493

[30] E. Oset and M. Rho; Phys. Rev. Lett. **42** (1979) 42

[31] I. S. Towner and F. C. Khanna; Phys. Rev. Lett. **42** (1979) 51

[32] A. Bohr and B. R. Mottelson; Phys. Lett. **B100** (1981) 10

[33] C. Gaarde; "Gamow–Teller Resonances", in Nuclear Physics, C. H. Dasso, R. A. Broglia and A. Winther (eds.) North–Holland, Amsterdam, (1982) p.347

[34] F. Osterfeld, D. Cha and J. Specht; Phys. Rev. **C31** (1985) 372

[35] J. Suhonen;Phys. Lett. **B255** (1991) 159

[36] H. Grawe, R. Schubart, K. H. Maier, D. Seweryniak, the OSIRIS and NORDBALL Collaborations; Physica Scripta **T56** (1995) 71

[37] M. Hencheck, R. N. Boyd, M. Hellström, D. J. Morrisey, M. J. Balbes, F. R. Chloupek, M. Fauerbach, C. A. Mitchell, R. Pfaff, C. F. Powell, G. Rainmann, B. M. Sherrill, M. Steiner, J. Vandegriff and S. J. Yennello; Phys. Rev. **C50** (1994) 2219

[38] M. Hencheck, R. N. Boyd and B. S. Meyer; Astrophys. J., in print

[39] M. Piiparinen, P. Kleinheinz, J. Blomquist, A. Virtanen, A. Atac, D. Mueller, J. Nyberg, T. Ramsoy and G. Sletten; Phys. Rev. Lett. **70** (1993) 150

[40] S. Flibotte, H. R. Andrews, G. C. Ball, C. W. Beausang, F. A. Beck, G. Belier, T. Byrski, D. Curien, P. J. Dagnall, G. de France, D. Disdier, G. Duchene, Ch. Finck, B. Haas, G. Hackmann, D. S. Haslip, V. P. Janzen, B. Kharraja, J. C. Lisle, J. C. Merdinger, S. M. Mullins, W. Nazarewicz, D. C. Radford, V. Rauch, H. Savajols, J. Styczen, Ch. Theisen, P. J. Twin, J. P. Vivien, J. C. Waddington, D. Ward, K. Zuber and S. Aberg; Phys. Rev. Lett. **71** (1993) 4299

[41] P. Kleinheinz, K. Zuber, C. Conci, C. Protop, J. Zuber, C. F. Liang, P. Paris and J. Blomquist; Phys. Rev. Lett. **55** (1985) 2664

[42] J. L. Tain, B. Rubio, P. Kleinheinz, D. Schardt, R. Barden and J. Blomqvist; Z. Phys. **A333** (1989) 29

[43] R. Menegazzo, P. Kleinheinz, R. Collatz, H. Gueven, J. Styczen, D. Schardt, H. Keller, O. Klepper, G. Walter, A. Huck, G. Marguier and J. Blomqvist; Z. Phys. **A349** (1994) 13

[44] W. Nazarewicz, J. Dobaczewski and T. R. Werner; Physica Scripta **T56** (1995) 9

[45] K. Grotz and H. V. Klapdor; "Die schwache Wechselwirkung in Kern-, Teilchen- und Astrophysik", Teubner, Stuttgart 1989

[46] E. Hagberg, V. T. Koslowsky, L. S. Towner, J. C. Hardy, J. G. Hykawy, G. Savard, T. Shinozuka, P. P. Unger and H. Schmeing; in Proc. of 6th Int. Conf. on Nuclei Far From Stability and 9th Int. Conf. on Atomic Masses and Fundamental Constants, Bernkastel-Kues 1992, R. Neugart, A. Wöhr (eds), IOP Conf. Ser. **132** (1993) 783 and refs. therein

[47] D. H. Wilkinson; Nucl. Instr. Meth. **A335** (1993) 172

[48] B. A. Brown and B. H. Wildenthal; At. Data and Nucl. Data Sheets **33** (1985) 347

[49] B. A. Brown and B. H. Wildenthal; Nucl. Phys. **A474** (1987) 290

[50] B. A. Brown and B. H. Wildenthal; Ann. Rev. Nucl. Part. Phys. **38** (1988) 29

[51] N. Auerbach, G. F. Bertsch, B. A. Brown, and L. Zho; Nucl. Phys. **A556** (1993) 190

[52] G. Walter; "Gamow-Teller Transitions: Progress and Problems", contribution to the Int. Conf. "Nuclear Shapes and Nuclear Structure at Low Excitation Energies",

Antibes, France, 20th–25th June, 1994, eds. M. Vergnes, D. Goutte, P. H. Heenen and J. Sauvage, Editions Frontieres 1994, p. 227

[53] K. Schmidt, T. W. Elze, R. Grzywacz, Z. Janas, R. Kirchner, O. Klepper, A. Płochocki, E. Roeckl, K. Rykaczewski, L. D. Skouras and J. Szerypo; Z. Phys. **A350** (1994) 99

[54] N. B. Gove and M. J. Martin; Nucl. Data Tables **10** (1971) 205

[55] B. S. Dzelepov, L. N. Zyryanova and Yu. P. Suslov; Beta Processes, Leningrad, Nauka, 1972

[56] J. C. Hardy, I. S. Towner, V. T. Koslowsky, E. Hagberg and H. Schmeing; Nucl. Phys. **A509** (1990) 429

[57] E. Klempt, P. Bobb, L. Hornig, J. Last, S. J. Freedman, D. Dubbers and O. Schärpf; Z. Phys. **C37** (1988) 179

[58] S. J. Freedman, Comments Nucl. Part. Phys. **19** (1990) 209

[59] B. G. Erozolimskii, I. A. Kuznetsov, I. V. Stepanenko, I. A. Kuida and Yu. A. Mostovoi; Phys. Lett. **B263** (1991) 33

[60] A. de Shalit and I. Talmi; "Nuclear Shell Theory", Academic Press, New York, London, 1963, p.59

[61] K. Rykaczewski, talk given during the Int. Conf. "New Nuclear Structure Phenomena in the Vicinity of Closed Shells" (SELMA'94); Stockholm, Sweden, 30th August–3rd September, 1994

[62] J. Blomqvist; "Gamow–Teller and First Forbidden Unique Transitions in the ^{132}Sn Region", contribution to the XXth Winter School "Selected Topics in Nuclear Structure", Zakopane, Poland, 13–26 April 1985

[63] Z. Szymański and J. Żylicz; in Proc. of International Symposium on Nuclear Physics of Our Times, Sanibel Island, USA, November 1992, ed. A. V. Ramaya, World Scientific 1993, p.100

[64] J. Dobaczewski, Z. Szymański and J. Żylicz; "Predictions for the ^{78}Ni →^{78}Cu Beta Decay", contribution to the Workshop on Nuclear Fission and Fission–Product Spectroscopy, Seyssins, France, May 1994; ILL Report 94FA05T, p. 190

[65] R. Kirchner, K. Burkard, W. Hüller and O. Klepper; Nucl. Instr. Meth. **186** (1981) 295

[66] H. L. Ravn; Proceedings of a Workshop on the ISOLDE Programme, B. W. Allardyce (ed.), Zinal, Switzerland, June 18th–22nd, 1981

[67] H. L. Ravn; Phys. Rep. **54** (1979) 201

[68] M. Huyse, P. Decrock, P. Dendooven, J. Gentens, G. Vancraeynest, P. Vandenberghe and P. van Duppen; Nucl. Instr. Meth. Phys. Res. **B70** (1992) 50

[69] R. Kirchner, K. Burkard, W. Hüller and O. Klepper; Nucl. Instr. Meth. Phys. Res. **B70** (1992) 56

[70] R. Kirchner; Nucl. Instr. Meth. Phys. Res. **B26** (1987) 204

[71] F. Scheerer, F. Albus, F. Ames, H.-J. Kluge and N. Trautmann; Spectrochim. Acta **B47** (1992) 793

[72] V. I. Mishin, V. N. Fedoseyev, H. J. Kluge, V. S. Lethokov, H. L. Ravn, F. Scheerer, Y. Schirakabe, S. Sundell and O. Tengblat; Nucl. Instr. Meth. Phys. Res. **B73** (1993) 550

[73] V. N. Fedoseyev, F. Albus, R. Kirchner, O. Klepper, H.-J. Kluge, V. I. Mishin, G. Paessler, E. Roeckl, F. Scheerer, K. Schmidt and N. Trautmann; "Study of Short–Lived Tin Isotopes with a Laser Ion Source"; contribution to the 7th Int. Symposium on Resonance Ionization Spectroscopy and Its Application, Bernkastel–Kues, Germany, 3rd–8th July, 1994, to be published by AIP

[74] M. Huyse, P. del Marmol, E. Coenen, K. Deneffe, P. van Duppen and J. Vanhorenbeeck; Z. Phys. **A330** (1988) 121

[75] G. Reusen, V. R. Bom, P. Decrock, P. Dendooven, M. Huyse, R. W. Hollander, P. van Duppen, J. Vanhorenbeeck and J. Wauters; Z. Phys. **A336** (1990) 381

[76] W. Reisdorf; Z. Phys. **A300** (1981) 227 and GSI Report **81–2** (1981) 73

[77] H. Stolzenberg, St. Becker, G. Bollen, F. Kern, H.-J. Kluge, Th. Otto, G. Savard, L. Schweikhard, G. Audi and R. B. Moore; Phys. Rev. Lett. **65** (1990) 3104

[78] G. Auger, W. Mittig, A. Lepine-Szily, L. K. Fifield, M. Bajard, E. Baron, D. Bibet, P. Bricault, J. M. Casandjian, M. Chabert, M. Chartier, J. Ferme, L. Gaudard, A. Gilibert, M. Lewitowicz, M. H. Moscatello, N. A. Orr, E. Plagnol, C. Ricault, A. C. C. Villari and Yang Yong Feng; Nucl. Instr. Meth. Phys. Res. **A350** (1994) 235

[79] B. Franzke; Nucl. Instr. Meth. **B24/25** (1987) 18 and GSI-Nachrichten **12-94** (1994) 7

[80] K. Rykaczewski, I. S. Grant, R. Kirchner, O. Klepper, V. T. Koslowsky, P. O. Larsson, E. Nolte, G. Nyman, E. Roeckl, D. Schardt, L. Spanier, P. Tidemand–Petersson, E. F. Zganjar and J. Żylicz; Z. Phys. **A322** (1985) 263

[81] H. Keller, R. Barden, R. Kirchner, O. Klepper, E. Roeckl, D. Schardt, I. S. Grant, A. Plochocki, K. Rykaczewski, J. Szerypo, J. Żylicz and the ISOLDE – Collaboration; Z. Phys. **A339** (1991) 355

[82] G.-E. Rathke, K. Rykaczewski, R. Kirchner, O. Klepper, V. T. Koslowsky, E. Roeckl, D. Schardt, I. S. Grant, P. O. Larson, A. Plochocki, J. Żylicz and P. Tidemand–Petersson; Z. Phys. **A321** (1985) 599

[83] H. Keller, R. Kirchner, O. Klepper, E. Roeckl, D. Schardt, R. S. Simon, P. Kleinheinz, R. Menegazzo, C. F. Liang, P. Paris, K. Rykaczewski and J. Żylicz; Z. Phys. **A340** (1991) 363

[84] H. Keller, R. Kirchner, O. Klepper, E. Roeckl, D. Schardt, R. S. Simon, P. Kleinheinz, C. F. Liang and P. Paris; Nucl. Instr. Meth. Phys. Res. **A300** (1991) 67

[85] D. Schardt, T. Batsch, R. Kirchner, O. Klepper, W. Kurcewicz, E. Roeckl and P. Tidemand–Petersson; Nucl. Phys. **A368** (1981) 153

[86] E. Roeckl and D. Schardt; "Recent Results on Alpha Radioactivity"; in Particle Emission from Nuclei, Vol. 2, CRC Press, Boca Raton, 1988, 1

[87] E. Roeckl; "Alpha Decay"; GSI Preprint **92–69** (1992), submitted for publication in "Handbook of Nuclear Decay Modes", IOP

[88] T. Faestermann, A. Gillitzer, K. Hartel, P. Kienle and E. Nolte; Phys. Lett. **B137** (1984) 23

[89] S. Hofmann; "Proton Radioactivity"; in Particle Emission from Nuclei, Vol. 2, CRC Press, Boca Raton, 1989, 25

[90] P. Graf and H. Münzel; Radiochim. Acta **20** (1973) 140

[91] K. Rykaczewski, R. Barden, H. Gabelmann, I. S. Grant, P. Hill, H. Keller, R. Kirchner, O. Klepper, A. Kolasiński, M. Pfützner, A. Płochocki, H. Ravn, E. Roeckl, D. Schardt, J. Szerypo, T. Thorsteinsten and J. Żylicz; Proceedings of XXI International Summer School on Nuclear Physics, Mikołajki 1990, Poland, A. Hilger (1991),p. 189

[92] B. Singh, H. W. Taylor, E. Browne, H. L. Hall, E. B. Norman, R. M. Larmier, A. O. Macchiavelli, K. T. Lesko and B. Sur; Z. Phys. **A341** (1992) 249

[93] K. Rykaczewski, A. Płochocki, I. S. Grant, H. Gabelmann, R. Barden, D. Schardt, J. Żylicz, G. Nyman and the ISOLDE – Collaboration; Z. Phys. **A332** (1989) 176

[94] J. Blachot, J. P. Husson, J. Oms and G. Berrier; Nucl. Data Sheets **37** (1984) 289

[95] R. Barden, R. Kirchner, O. Klepper, A. Płochocki, G.-E. Rathke, E. Roeckl, K. Rykaczewski, D. Schardt and J. Żylicz; Z. Phys. **A329** (1988) 319

[96] J. Szerypo, R. Barden, L. Kalinowski, R. Kirchner, O. Klepper, A. Płochocki, E. Roeckl, K. Rykaczewski, D. Schardt and J. Żylicz; Nucl. Phys. **A507** (1990) 357

[97] P. de Gelder, E. Jacobs, D. de Frenne; Nucl. Data Sheets **38** (1983) 545

[98] M. Lewitowicz, R. Anne, G. Auger, D. Bazin, M. G. Saint–Laurent, R. Grzywacz, M. Pfützner, K. Rykaczewski, J. Żylicz, S. Lukyanov, A. Fomichov, Yu. Penionzhkevich, O. Tarasov, V. Borrel, D. Guillemaud–Mueller, A. C. Mueller, H. Keller, O. Sorlin, F. Pougheon, M. Huyse, T. Pluym, J. Szerypo, J. Wauters, C. Borcea, K. Schmidt and Z. Janas; Nouvelles du GANIL **48**, December 1993 (1993) 7

[99] A. Johnson, D. Seweryniak, B. Cederwall, J. Nyberg, A. Atac, J. Blomquist, J. Cederkall, C. Fahlander, M. Karny, A. Kerek, J. Kownacki, L.-O. Norlin,

R. Wyss, E. Adamides, H. Grawe, E. Ideguchi, R. Julin, S. Juutinen,
W. Karczmarczyk, S. Mitarai, M. Piiparinen, R. Schubart, G. Sletten, S. Tormanen
and A. Virtanen; Nucl. Phys. **A557** (1993) 401c

[100] R. Schneider, T. Faestermann, J. Friese, R. Gernhauser, H. Gilg, F. Heine,
J. Homolka, P. Kienle, H. J. Körner, J. Reinhold, K. Zeitelhack, H. Geissel,
G. Münzenberg and K. Sümmerer; Physica Scripta, **T56** (1995) 67

[101] R. Barden, D. Boyd, C. Bruske, K. H. Burkard, W. Hüller and D. Schardt;
GSI Scientific Report 1986, GSI Rep. **87–1** (1987) 278
R. Barden; Thesis, Johannes–Gutenberg Universität, Mainz 1988
and GSI Preprint **88–18** (1988)

[102] T. Elmroth, E. Hagberg, P. G. Hansen, J. C. Hardy, B. Jonson, H. L. Ravn and
P. Tidemand–Petersson; Nucl. Phys. **A304** (1978) 493

[103] Z. Janas, H. Keller, R. Kirchner, O. Klepper, A. Piechaczek, E. Roeckl, K. Schmidt,
M. Huyse, J. von Schwarzenberg, J. Szerypo, P. Van Duppen, L. Vermeeren,
F. Albus, H.–J. Kluge, G. Paessler, F. Scheerer, N. Trautmann, V. N. Fedoseyev,
V. I. Mishin, R. Grzywacz, A. Plochocki, K. Rykaczewski, J. Żylicz; Physica Scripta
T56 (1995) 262

[104] G. Audi and A. H. Wapstra; Nucl. Phys. **A565** (1993) 1

[105] P. Tidemand–Petersson, R. Kirchner, O. Klepper, W. Kurcewicz, E. Roeckl and
E. F. Zganjar; Z. Phys. **A302** (1981) 343

[106] J. Szerypo, M. Huyse, G. Reusen, P. Van Duppen, H. Keller, R. Kirchner,
O. Klepper, E. Roeckl, D. Schardt, R. Grzywacz, M. Pfützner, A. Plochocki,
K. Rykaczewski, J. Żylicz, G. Alkhazov, L. Batist, A. Bykov, V. Wittmann and
B. A. Brown; Nucl. Phys. **A584** (1995) 221

[107] M. Pfützner, A. Plochocki, K. Rykaczewski, J. Szerypo, J. Żylicz, H. Keller,
R. Kirchner, O. Klepper, E. Roeckl, D. Schardt, M. Huyse, G. Reusen,
P. van Duppen and A. Brown; Nucl. Phys. **A581** (1995) 20

[108] S. Shastry, H. Bakhru and I. M. Ladenbauer-Bellis; Phys. Rev. **C1** (1970) 1835

[109] D. de Frenne and E. Jacobs; Nucl. Data Sheets **68** (1993) 935

[110] J. Blachot; Nucl. Data Sheets **62** (1991) 709

[111] L. Batist, V. Wittmann, G. Alkhazov, A. Bykov, H. Keller, R. Kirchner, E. Roeckl, P. van Duppen, M. Huyse, G. Reusen, A. Płochocki, M. Pfützner, K. Rykaczewski, J. Szerypo and J. Żylicz; GSI Scientific Report 1992, GSI **93-01** (1993) 82

[112] L. Batist, A. Bykov, F. Moroz, V. Wittmann, G. Alkhazov, H. Keller, R. Kirchner, O. Klepper, E. Roeckl, M. Huyse, P. Van Duppen, G. Reusen, A. Płochocki, M. Pfützner, K. Rykaczewski, J. Szerypo, J. Żylicz and B. A. Brown; Z. Phys. **A351**, (1995) 149

[113] B. Singh and J. A. Szucs; Nucl. Data Sheets **60** (1990) 1

[114] S. Ćwiok, J. Dudek, W. Nazarewicz, J. Skalski and T. Werner; Comp. Phys. Comm. **46** (1987) 379

[115] J. Dudek, A. Majhofer, J. Skalski, T. Werner, S. Ćwiok and W. Nazarewicz; J. Phys. **G5** (1979) 1359

[116] J. Dudek, Z. Szymański and T. Werner; Phys. Rev. **C23** (1981) 920

[117] V. M. Strutinsky; Nucl. Phys. **A95** (1967) 420

[118] P. Möller and J. R. Nix; At. Data and Nucl. Data Tables **26** (1981) 165

[119] H. J. Lipkin; Ann. Phys. (N.Y.) **9** (1960) 272

[120] Y. Nogami; Phys. Rev. **B134** (1964) 313

[121] Y. Nogami and I. J. Zucker; Nucl. Phys. **60** (1964) 203

[122] H. C. Pradhan, Y. Nogami and J. Law; Nucl. Phys. **A201** (1973) 357

[123] G. Ulm, J. Eberz, G. Huber, H. Lochmann, R. Menges, R. Kirchner, O. Klepper, T. Kuhl, P. O. Larsson, D. Marx, D. Murnick and D. Schardt; Z. Phys. **A321** (1985) 395

[124] J. Eberz, U. Dinger, G. Hubert, H. Lochmann, R. Menges, R. Neugart, R. Kirchner, O. Klepper, T. Kuhl, D. Marx, G. Ulm and G. Wendt; Nucl. Phys. **A464** (1987) 9

[125] L. Kalinowski; "Structure of 1^+ States in Neutron Deficient Odd–Odd Indium Isotopes", Proceedings of the International Workshop, Bad Honnef, Federal Republic of Germany, April 24–28, J. Eberth et al. (eds), Springer–Verlag 1988, 397

[126] J. Van Maldeghem and K. Heyde; Phys. Rev. **C32** (1985) 1067

[127] D. H. Gloeckner and F. J. Serduke, Nucl. Phys. **A220** (1974) 477

[128] H. Kruse and B. H. Wildenthal, Bull. Am. Phys. Soc. **27** (1982) 725

[129] A. Hosaka, K. I. Kubo and H. Toki, Nucl. Phys. **A244** (1985) 76

[130] K. Rykaczewski; talk given at Warsaw University, 8 Dec. 1993

[131] A. Piechaczek, M. F. Mohar, R. Anne, V. Borrel, B. A. Brown, J. M. Corre, D. Guillemaud–Mueller, R. Hue, H. Keller, S. Kubono, V. Kunze, M. Lewitowicz, P. Magnus, A. C. Mueller, T. Nakamura, M. Pfützner, E. Roeckl, K. Rykaczewski, M. G. Saint-Laurent, W.-D. Schmidt–Ott and O. Sorlin; "Beta–Decay of ^{20}Mg", Nucl. Phys. **A584** (1995) 509

[132] W. Trinder, E. G. Adelberger, Z. Janas, H. Keller, K. Krumbholz, V. Kunze, P. Magnus, F. Meissner, A. Piechaczek, M. Pfützner, E. Roeckl, K. Rykaczewski, W.-D. Schmidt-Ott and M. Weber; Phys. Lett. **B349** (1995) 267

[133] W. Trinder, E. G. Adelberger, Z. Janas, H. Keller, K. Krumbholz, V. Kunze, P. Magnus, F. Meissner, A. Piechaczek, M. Pfützner, E. Roeckl, K. Rykaczewski, W.-D. Schmidt-Ott and M. Weber; Phys. Lett. **B348** (1995) 331

[134] P. Hornshoj, K. Wilsky, P. G. Hansen, B. Jonson and O. B. Nielsen; Nucl. Phys. **A187** (1972) 609

[135] Z. Janas, G. D. Alkhazov, L. Batist, R. Bonnetti, B. A. Brown, A. Bykov, Th. W. Elze, R. Grzywacz, A. Guglielmetti, M. Huyse, H. Keller, R. Kirchner, O. Klepper, M. Pfützner, A. Piechaczek, A. Płochocki, G. Poli, P. B. Price, E. Roeckl, G. Reusen, K. Rykaczewski, D. Schardt, K. Schmidt, J. von Schwarzenberg, L. D. Skouras, J. Szerypo, P. Van Duppen, L. Vermeeren, V. Wittmann, and J. Żylicz; 'Decay Studies near ^{100}Sn', contr. to ENAM conference, Arles, France, 18th-23rd June, 1995

[136] B. Jonson, E. Hagberg, P. G. Hansen, P. Horshoj and P. Tidemand–Petersson; in Proc. 3rd Int. Conf. on Nuclei far from Stability, Cargese, France, 1976, CERN 76-13, p. 277

[137] E. Roeckl; "Recent Experiments on Proton, Alpha and Cluster Radioactivity"; in Proc. of the Int. Conf. "Cluster in Nuclear Structure and Dynamics" (CLUSTER'94), Strasbourg, 6th–9th September, 1994, Editions Frontieres, in print

[138] A. Guglielmetti, B. Blank, R. Bonetti, Z. Janas, H. Keller, R. Kirchner, O. Klepper, A. Piechaczek, A. Plochocki, G. Poli, P. B. Price, E. Roeckl, K. Schmidt, J. Szerypo and A. J. Westphal; "Production of ^{114}Ba in ^{58}Ni+^{58}Ni reactions and detection of its cluster radioactivity", contribution to the Proc. of the fifth Int. Conf. on Nucleus–Nucleus Collisions, Taormina, Italy, 30th May–4th June, 1994; Nucl. Phys. **A583** (1995) 867c

[139] J. M. Nitschke, K. Burkard, W. Hüller, R. Kirchner E. Roeckl, M. Karny, S. Lewandowski and A. Sulik; "The Total–Absorption Spectrometer (TAS) at the On-line Mass Separator", GSI Annual Report 1994 **GSI–95–1**, p. 285

[140] R. Kirchner and V. I. Mishin; private communication 1994

[141] G. Auger, W. Mittig, A. Lepine-Szily, M. Chartier, D. Bibet, J. M. Casandjan, M. Chabert, J. Ferme, A. Gilibert, M. Lewitowicz, M. Mac Cormick, M. H. Moscatello, N. A. Orr, E. Plagnol, C. Ricault, C. Spitaels and A. C. C. Villari; Nouvelles du GANIL **54** (1995) 11